A THESIS SUBMITTED TO
THE GRADUATE SCHOOL OF NATURAL AND APPLIED SCIENCES
OF ÇANKIRI KARATEKİN UNIVERSITY

IMPROVING MAXIMUM POWER POINT TRACKING MPPT USING DIFFERENT CONTROLLER TECHNIQUES

IN PARTIAL FULFILLMENT OF THE REQUIREMENTS
FOR
THE DEGREE OF MASTER OF SCIENCE
IN
ELECTRICAL AND ELECTRONICS ENGINEERING

BY

AHMED RASHID MADGHASH AL-JABARI

ÇANKIRI

2022

IMPROVING MAXIMUM POWER POINT TRACKING MPPT USING DIFFERENT CONTROLLER TECHNIQUES

By Ahmed Rashid Madghash AL-JABARI

June 2022

We certify that we have read this thesis and that in our opinion it is fully adequate, in scope and in quality, as a thesis for the degree of Master of Science

Advisor **:** Assoc. Prof. Dr. Fatih KORKMAZ

Examining Committee Members:

Chairman **:** Assoc. Prof. Dr. Nihat DALDAL
Electrical - Electronics Engineering
Bolu Abant İzzet Baysal University

Member **:** Assoc. Prof. Dr. Fatih KORKMAZ
Electrical - Electronics Engineering
Çankırı Karatekin University

Member **:** Asst. Prof. Dr. Göksu GÖREL
Electrical - Electronics Engineering
Çankırı Karatekin University

Approved for the Graduate School of Natural and Applied Sciences

Prof. Dr. İbrahim ÇİFTÇİ
Director of Graduate School

I hereby declare that all information in this document has been obtained and presented in accordance with academic rules and ethical conduct. I also declare that, as required by these rules and conduct, I have fully cited and referenced all material and results that are not original to this work.

Ahmed Rashid Madghash AL-JABARI

ABSTRACT

IMPROVING MAXIMUM POWER POINT TRACKING MPPT USING DIFFERENT CONTROLLER TECHNIQUES

Ahmed Rashid Madghash AL-JABARI
Master of Science in Electrical and Electronics Engineering
Advisor: Assoc. Prof. Dr. Fatih KORKMAZ
June 2022

As it is known that, one of the obvious disadvantages of a photovoltaic system is the low power output of solar radiation because of the changes in the environmental conditions. An inexpensive and practical solution related to convert a solar energy is tracking the maximum power point of the solar panel. The project reviews the methods for finding the maximum power point based on the perturbation of the photovoltaic system. A comparative analysis of the methods is carried out, their advantages and disadvantages are revealed. The mathematical model of the system and the algorithms were reviewed and a complete model was built in the Matlab environment and the results were presented. An example of the construction of an analog control system for a DC voltage converter of a hysteresis type is shown. The work of a solar battery in conditions of partial shading, which leads to difficulties in tracking the global maximum power point, and ways of solving this problem are considered. The study focused on three common techniques in tracking MPPT, Perturb and Observe P&O, Incremental Conductance IC and Fuzzy Logic Control FLC. For fast charging and increasing the battery life cycle, PI controller was added and connected with the DC-DC converter.

2022, 75 pages

Keywords: Point of maximum power, Photovoltaics, Solar battery, DC voltage converter, Partial shading, Control system

ÖZET

FARKLI DENETLEYİCİ TEKNİKLERİ KULLANARAK MAKSİMUM GÜÇ NOKTASI İZLEME MPPT'SİNİN İYİLEŞRİTİLMESİ

Ahmed Rashid Madghash AL-JABARI
Elektrik ve Elektronik Mühendisliği, Yüksek Lisans
Tez Danışmanı: Doç. Dr. Fatih KORKMAZ
Haziran 2022

Bilindiği gibi, bir fotovoltaik sistemin bariz dezavantajlarından biri, çevresel koşullardaki değişikliklerden dolayı güneş radyasyonunun düşük güç çıkışıdır. Güneş enerjisini dönüştürmek için ucuz ve pratik bir çözüm, güneş panelinin maksimum güç noktasını izlemektir. Proje, fotovoltaik sistemin bozulmasına dayalı olarak maksimum güç noktasını bulma yöntemlerini gözden geçirmektedir. Yöntemlerin karşılaştırmalı bir analizi yapılır, avantajları ve dezavantajları ortaya çıkar. Sistemin matematiksel modeli ve algoritmalar gözden geçirilerek, Matlab ortamında eksiksiz bir model oluşturulmuş ve sonuçlar sunulmuştur. Histerezis tipi bir DC voltaj dönüştürücü için bir analog kontrol sisteminin yapımına bir örnek gösterilmektedir. Küresel maksimum güç noktasının izlenmesinde zorluklara yol açan kısmi gölgeleme koşullarında bir güneş pilinin çalışması ve bu sorunu çözme yolları ele alınmaktadır. Çalışma, MPPT, Perturb and Observe P&O, Artımlı İletkenlik IC ve Fuzzy Logic Control FLC takibinde yaygın olarak kullanılan üç tekniğe odaklandı. Hızlı şarj etmek ve pil ömrünü artırmak için PI denetleyici eklendi ve DC-DC dönüştürücü ile bağlandı.

2022, 75 sayfa

Anahtar Kelimeler: Maksimum güç noktası, Fotovoltaik, Güneş pili, DC voltaj dönüştürücü, Kısmi gölgeleme, Kontrol sistemi

PREFACE AND ACKNOWLEDGEMENTS

Throughtout time, although of difficulties of live and finding an enough time to study and enhance my knowledge in my academic specialization, we could achieve one of my important ambitions, I became aware that we can achieve the goal anywhere and anytime just we need to not giving up on lofty goals, no matter how long just need to seize the opportunities and be brave and begin your adventure.

On this occasion, I would like firstly to thank my suppurvisor and thesis advisor, Asst. Prof. Dr. Fatih KORKMAZ, for his patience, guidance and understanding. Also, thank my family and particulary my wife for supporting all the time.

Ahmed Rashid Madghash AL-JABARI

Çankırı-2022

CONTENTS

LIST OF SYMBOLS

C	Capacitance
D	Duty ratio
I	Current of solar cell
I_D	Diode current
I_{mpp}	Current at maximum power point
I_o	Reverse saturation current of diode
I_{in}	Input current of PV system
I_{out}	Output current of PV system
I_{ph}	Photocurrent
I_r	Irradiance
I_{Rp}	Current flowing through the equivalent parallel resistance
I_{sat}	Diode saturation current
I_{sc}	Short circuit Current
K	Boltzmann's Constant
L	Inductance
P	Power
P_{HScond}	Power loss equations for the HS-MOSFET
P_{SW_HS}	Switching losse
P_{VFD}	Forward conduction loss of diode
q	Electron charge constant
Q_{SW}	Switching charge
R	Resistance
R_{Gate}	Total resistance in the gate drive path
R_p	The equivalent parallel resistance
R_{thJC}	The thermal package resistance
T	Temperature
V	Voltage
V_{mpp}	Voltage at maximum power point
V_{oc}	Open circuit voltage
V_{in}	Input voltage
V_{out}	Output voltage
γ	Duration of the open state of the power switch of the voltage

LIST OF ABBREVIATIONS

CVC	Current-voltage characteristic
DC	Direct current
dI	Derivative of current
dP	Derivative of power
dV	Derivative of voltage
FLC	Fuzzy logic control
IC	Incremental conductance
MPP	Maximum power Point
MPPT	Maximum power point tracking
P&O	Perturbation and observation
PS	Partial shading
PV	Photovoltaic
PWM	Pulse width modulation
STC	Standard test condition

LIST OF FIGURES

LIST OF TABLES

1 INTRODUCTION

1.1 Rationale of the Study

It is known that worldwide power consumption rises every year, and further growth is expected to be driven by population growth and the increasing demands of modern lifestyles. Increasing demand for electricity is rapidly depleting traditional fossil fuels and exacerbating the problem of environmental pollution. As a result, alternative (renewable) energy sources must be developed in order to assure long-term energy supplies to consumers while also reducing local and global pollution. Solar energy is one of the most acceptable sources of power generation since it is infinite, entirely free (in terms of availability), and ecologically beneficial. Many countries are moving to the use of photovoltaic (PV) systems for generating electrical power, even at their high cost.

Although considerable efforts have been achieved in improving PV cell technology throughout the history of photovoltaics, the total efficiency of the solar module remains low. There is a single point with coordinates (Vmpp, Impp) on the current-voltage characteristic (CVC) of the solar module where its output power reaches its maximum (Figure 1.1). Therefore, to achieve the maximum efficiency of a solar module when constructing a PV system, it is necessary to use an algorithm for tracking the maximum power point), in order to transfer to the load the maximum possible power of the solar module under the given conditions. Achieving this task is complicated by the nonlinear dependence of the current generated by the solar module on its output voltage, the dependence of the generated power on solar radiation and temperature, and the problem of partial shading of modules (PS - partial shading) that make up the solar battery (Tajuddin *et al.* 2015). Numerous MPPT methods of varying complexity are described in foreign literatüre (Babaa *et al.* 2014, Faranda and Leva 2008).

The commercial products that are most commonly utilized including perturbation and observation (P&O) and incremental conductance (IC) methods (Dolara *et al.* 2009, Femia *et al.* 2006) because of their simple control structures as well as ease of implementation.

For PV systems with a low level of tracking accuracy of MPPT, methods such as constant voltage (CV) and current (Leedy *et al.* 2012, Pandey *et al.* 2007, Xiong *et al.* 2012), short-current pulse (SC) (Park and Yu 2004) , open circuit voltage (OC) are used (Lopez-Lapena and Penella 2012). These methods require only fewer sensors and are low-cost to implement. Methods of searching for MPPT based on computational intelligence (CI) have grown popular with the advancement of computer technology due to their adaptive nature, which is extremely successful while working in conditions of partial shade of solar modules and rapid changes in illumination. Generally, CI methods can be divided to Artificial intelligence (AI) and evolutionary computation (EC) approaches.

All the algorithms considered in the project are based on finding an extremum on the current-voltage characteristic of a photoelectric converter. The implementation of the most common methods of tracking the maximum power point is considered: "Disturbance and observation" and "Increase in conductivity". An algorithm based on fuzzy logic theory is proposed to improve the efficiency of photovoltaic cells as an alternative to traditional algorithms. The solar panel control system model is implemented in MATLAB / Simulink. Three methods of tracking the maximum power point in this photovoltaic system are considered and implemented. A comparative analysis of the operation of various control algorithms for different levels of solar radiation intensity is carried out. Practical significance algorithms can be implemented in real power systems to improve their overall performance.

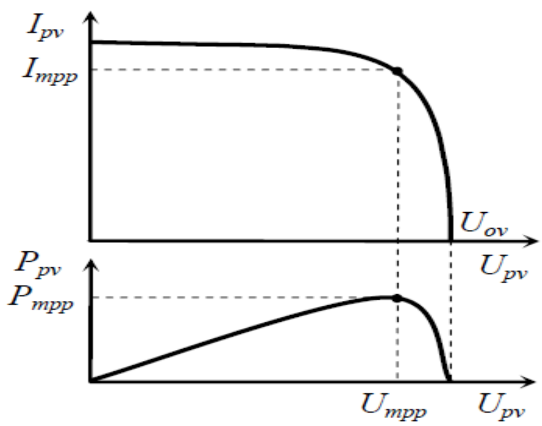

Figure 1.1 Solar module static characteristics

1.2 Motivation

Alternative energies and benefiting from them are among the most important topics being studied, developed and implemented at the present time. Therefore, this project was implemented because of its importance in practical life and to gain knowledge that can be used for future research work. The work on this project also made it possible to identify several algorithms that are widely used at the present time, and they proved practical and effective, and the comparison between them allowed for an accurate understanding of the work.

Because of that, P&O based MPPT method has an oscillation problem in steady states which is unavoidable, the motivation behind this project is to improve the maximum power point tracking by implementing different techniques based MPPT method.

1.3 Contribution

In this work, the theoretical study and the identification of algorithms for optimizing the maximum power point tracking MPPT using different console techniques were simulated in MATLAB environment and the results of different algorithms were reviewed. We can summarize the contribution as following:

- Taking an overview of the characteristics of the PV model and related parameters with MPPT.
- Modeling the system completely by finding a model for each of its components.
- System simulation in MATLAB environment.
- Comparing among the performance of algorithms based on simulation results

2 LITERATURE REVIEW

A few MPPT procedures in conjunction with their usage are detailed within the writing (Balagurov *et al.* 2015, Lee *et al.* 2006). Researchers are frequently perplexed whereas selecting an MPPT procedure for a specific application. Shockingly, as there were many strategies available in this field counting Bend fitting, Fragmentary Brief Circuit Current, Fragmentary Open Circuit Voltage, See Up Table, One Cycle Control, Irritate and Watch, Incremental Conductance and Input methods prior that incorporates discourses on MPPT strategies until 2007 (Esram *et al.* 2006, Salas *et al.* 2005).

Numerous modern MPPT strategies have been detailed since at that point outlined in other papers (De Cesare *et al.* 2006, Kottas *et al.* 2006). Among all the MPPT strategies, Irritate & Watch (P&O) and Incremental Conductance (IC) are most popular used because of their straightforward usage and lesser time for tracking the most extreme control point conjointly other financial reasons. Under all of a sudden changing climate conditions (illumination level) as MPP changes persistently, P&O takes it as a alter in MPP due to irritation instead of that of illumination and now and then closes up in calculating off-based MPP (Elgendy *et al.* 2011).

It has been watched that the productivity of the framework moreover depends upon the converter. For the most part, it is greatest for a buck analysis, at that point for buck-boost examination and least for a boost examination (Kobayashi *et al*. 2004). When numerous sun based modules are associated in parallel, equalization of yield working focuses in correspondence to constrain uprooting of input working focuses of the identical working framework is assessed. It is exceptionally basic to carry out and has tall effectiveness both beneath stationery and time shifting barometrical conditions (Tajuddin *et al.* 2015) .

Among all the MPPT strategies (Jusoh *et al.* 2018, Kchaou *et al.* 2016), Annoy & Watch (P&O) and Incremental Conductance are most commonly utilized since of their straightforward usage and lesser time for tracking the most extreme power point conjointly other financial reasons. Beneath abruptly changing climate conditions (light level) as MPP changes continuously, P&O takes it as a alter in MPP due to irritation instead of that of illumination and some of the time closes up in calculating off-base MPP (Esram and Chapman 2007) . Since the most extreme sum of sun-based vitality, captured by the collector, is related to the exactness for following sun's position (Tremblay *et al.* 2007) , at that point a high-precision sun following controller ought to be considered.

In past a long time, some plans have been proposed to make strides following frameworks for taking after the direction of the sun based on introduction and tilt movement control (Esram and Chapman 2007, Salas *et al.* 2006). These plans incorporate: optimizing tilt and introduction points of sun-oriented collectors by utilizing topographical latitudes information (Femia *et al.* 2005), scientific models (Leedy *et al.* 2012), and following calculations (Lopez-Lapena and Penella 2012, Narendiran *et al.* 2013). In arrange to naturally alter tilt and orientation points in connection to the sun position, within the field of control building a few approaches have proposed based on the movement control (Kato and Koizumi 2015, Patel and Agarwal 2008) and flag handling by utilizing data coming from electronic gadgets (Koutroulis and Blaabjerg 2012, Pandey *et al.* 2007).

Finllay, there are alot of studies (Abo-Sennah *et al.* 2021, Babaa *et al.* 2014, Dolara *et al.* 2009, Dorofte *et al.* 2005, Esram and Chapman 2007, Selvan and Kumar 2015) worked on the comparsion among the MPPT techniques such as our case study but no extensive study including improving the MPP with diversity of teqniques in a one study where the majority of them are concentrating on one or two improvments as a maximum level.

3 MATHEMITACAL MODELLING

Presented in this section the mathematical model of whole the system, which consists of four subsystems, as described below:

- The first one is the PV, which is represented by its equations.
- The model of DC- DC converter.
- The equations that describe the MPPT methods.
- And finally, the battery model.

3.1 Modelling of a PV Array

A PV grid uses one or more PV arrays for converting solar energy into electrical energy. The elementary unit of a PV array is a PV cell and it works on photovoltaic principle (Haque 2014, Ngan and Tan 2011). Photovoltaic effect can be defined as conversion of light into electrical energy by means of outer electrons that break the bond in a semiconductor device when the photon energy is higher than the band gap energy. The photoelectric effect is at the core of the operation of the solar cell, the photocell converts photon energy into electrical energy. In order to determine the relationship between the output voltage and current of the solar panel, we use the equivalent circuit as in Figure 3.1.

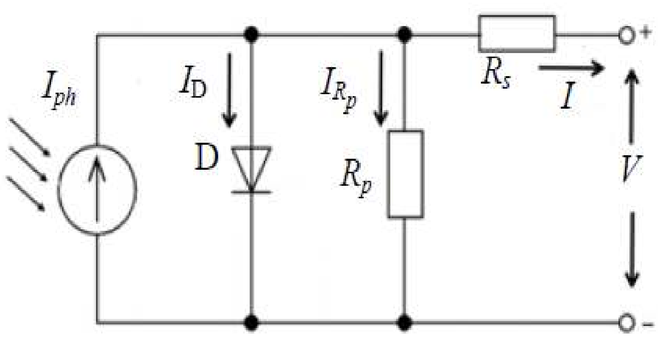

Figure 3.1 Solar panel equivalent circuit

As in (Karlsson *et al.* 2018, Pathak and Yadav 2019), the relationship between the output current and voltage, in accordance with this scheme, could be represented as follows Equation (3.1):

$$I = I_{ph} - I_D - I_{R_p} = I_{ph} - I_{sat}\left(\exp\left[\frac{q(V+IR_s)}{AKT}\right] - 1\right) - \frac{(V+IR_s)}{R_p} \qquad (3.1)$$

Where;

I_{ph}: the photo current.

I_D: the diode current.

I_{R_p}: the current flowing through the equivalent parallel resistance.

I_{sat}: the diode saturation current.

R_s: the equivalent series resistance

R_p: the equivalent parallel resistance.

V: the output voltage.

I: the output current.

q: the electron charge (1.602 $*10^{-19}$ C).

A: the coefficient of "ideality".

k: the Boltzmann coefficient (1.381$*10^{-23}$ J/K).

T: the ambient temperature.

A PV cell consists of semiconductor diode whose Shockley diode equation is given by Equation (3.2):

$$I_D = I_{sat}\left[\exp\left(\frac{qV_{PV}}{AKT}\right) - 1\right] \qquad (3.2)$$

It is known that the photocurrent I_{ph}, and hence the output current and voltage, depend on solar radiation and temperature. The maximum power is achieved at a certain voltage. In order for the solar cell to produce maximum power, it is necessary to regulate the output voltage and load resistance. To do this, it is necessary to install a power converter between the electrical installation and the load (Al-Majidi *et al.* 2018, Zhou *et al.* 2010).

3.2 DC-DC Buck Converter

A buck converter is the foremost essential Switch Mode Control Supply (SMPS) topology. It is broadly utilized the industry to change over the next input voltage into a lower output voltage. The buck converter (voltage step-down converter) may be a non-isolated converter, subsequently galvanic separation between input and output isn't given.

The foremost well known topology utilized to convey control in complex systems; it gives the desired nearby voltage from a better voltage transport that's common to numerous converters within the framework. The converter itself comprises of one dynamic switch controlled by an IC, a rectifier and channel components. This extraordinary effortlessness permits for fetched successful tall effective control dispersion all through the application (Chauhan *et al.* 2013, Sharma and Jain 2014).

The buck converter has the filter inductor on the yield side, which gives a smooth ceaseless yield current waveform to the stack as presented in Figure 3.2. This may well be considered a qualitative benefit but requires uncommon contemplations for enormous stack drifters. The input is uncovered to the transistor (SW). In this manner, the input current may be a exceedingly energetic waveform. This is often undesired as the exchanged current radiates commotion into the complete framework.

The following four parameters should be calculated in the power stage:

- Calculation of Input voltage range V_{in}(min) and V_{in} (max).
- Calculation of Nominal output voltage V_o.
- Calculation of Maximum output current I_o (max).

In the event that an integrated circuit as shown in Figure 3.2 is used to build a buck converter, it is necessary to choose the parameters according to the technical bulletin of the integrated circuit in order to accurately determine the performance of the buck converter and determine the power spent in it.

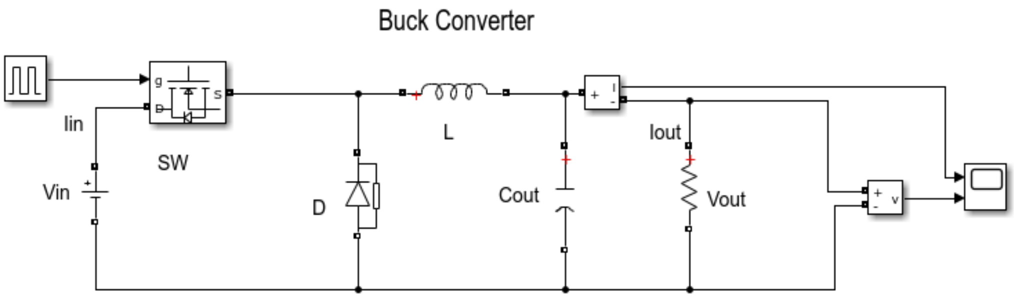

Figure 3.2 DC-DC buck converter model

The taking after are plan conditions for the CCM worked buck. A plan case has been calculated together with the depiction (Table 3.1).

Table 3.1 DC-DC Specifications

Input voltage	29 V
Out voltage	12.5 V
Switching frequency	10 KHz
Inductor current ripple ΔI_L	$0.1*I_o = 0.734$
Output rated power	10 W
Maximum power	213 W
Voltage ripple	< 20 mv

3.2.1 Filters of inductor and capacitor

The filter peak current, and its inductor value as explained in Figure 3.3 are calculated based on the particular maximum inductor current ripple (Atallah *et al.* 2014, Sharma and Jain 2015).

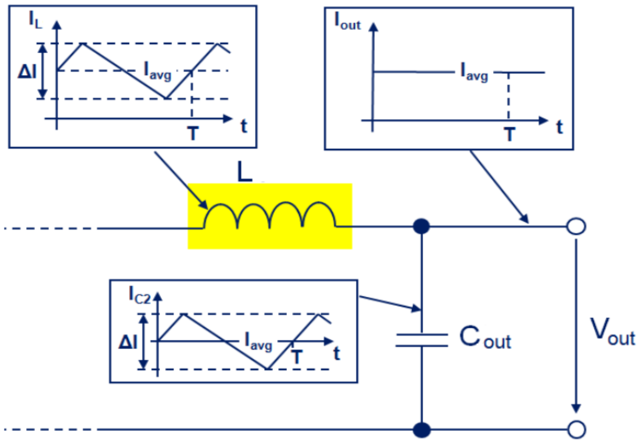

Figure 3.3 Filter inductor and its signals

For a DC-DC buck convertor, a duty cycle can be extracted from the following Equation (3.3):

$$D = \frac{\mathrm{V_o}}{\mathrm{V_{in}}} \tag{3.3}$$

The filter of inductor could be expressed as Equation (3.4), Equation (3.5):

$$V_L = L\frac{di_L}{dt} = L\frac{\Delta I_L}{(1-D)T}V_o \tag{3.4}$$

$$L = \frac{V_o(V_{in}-V_o)}{V_{in}f_{sw}\Delta I_L} \tag{3.5}$$

While the capcitor filter could be calculated from the following Equation (3.6):

$$C = \frac{\Delta I_L}{8f_{sw}\Delta V_r} \tag{3.6}$$

From parameters given in Table 3.1, the theortical values of inductor, capacitor in addation to the duty cycle (Yilmaz *et al.* 2018) have to be:

- L=1.9 mH
- C=0.1469 mF
- D=0.431

Changing the duty cycle based on power loss in high-efficiency converters usually does not have much effect on the inductor value and it can be ignored when choosing an inductor. Then the peak current of the inductor is Equation (3.7), Equation (3.8):

$$I_{pk} = I_o + \frac{\Delta I_L}{2} \tag{3.7}$$

$$I_{pk} = I_o + \frac{0.1 * I_{out}}{2} = 1.05 I_o = 1.05 * 7.3445 = 7.711 A \tag{3.8}$$

For this situation, the inductor must be able to handle a peak current of 7.711 A without saturation. An important point that the inductor retains its inductance at the elevated operating temperatures depending on the PV temperature and the inductor losses, which consist of core losses and DCR losses.

3.2.2 Rectifire

The forward conduction loss of the rectifier diode D1 can be calculated in Equation (3.9):

$$P_{VFD} = V_{FD} I_o (1 - D) = 0.7 * 7.3448 * (1 - 0.414) = 3.01\ W \tag{3.9}$$

Because of the various dependencies, determining the switch recovery misfortune from the datasheet is quite difficult. However, in the case of state-of-the-art MOSFETs, it is so little that it is unlikely to have a significant role in MOSFET selection. A few MOSFETs have been implanted with inversion recovery mechanisms that bypass the body diode. At the expense of RDSON per kick the bucket region, those FETs have an edge on switch recuperation misfortune. The driver that controls the door of swapping FET and synchronous rectifier MOSFET with the least time between them is a fundamental criterion for reducing dead time disaster. The swapping frequency is directly proportional to the dead time misery as in the equation below Equation (3.10):

$$P_{tdead} = V_{FSync} I_o (t_{deadH} + t_{deadL}) f_{sw} \tag{3.10}$$

For the case here it expects a exchanging recurrence of 5kHz and a dead time per move of 10ns. The forward voltage drop over the body diode is accepted to be 0.8V as in Equation (3.11):

$$P_{tdead} = 0.8 * (7.3448 * (10ns + 10ns)5kHz) = 0.6\ mW \tag{3.11}$$

The driving voltage VGS drive is another basic operation parameter. It impacts the RDSON and exchanging speed of the MOSFET. Entryway charge of the MOSFET and its RDSON are conversely corresponding to each other in a given innovation. Subsequently, an ideal MOSFET depends moreover on the chosen switching frequency and gate drive voltage.

3.2.3 Switching MOSFET

The buck converter could be a topology of hard-switched. The exchanging MOSFET ought to work as an perfect switch (being moo ohmic and quick exchanging). As with the synchronous rectifier MOSFET (Elbaksawi 2019), the FOM is setting limits to as distant one can come to a perfect switch.

For a buck converter switch, the following are major MOSFET selection criteria;

1. Low FOMs for - RDSON·QG and RDSON·Qoss
2. Ratio $\frac{Q_{GD}}{Q_{GS}} < 1$ for immunity against dv/dt induced turn-on
3. The ON/OFF switching is fast, the working point is near middle of gate drive range

4. At the desired point of peak efficiency the switching and conduction losses must be balanced for a minimum overall loss.
5. Handle spikes which is caused by voltage overshoot using VDS rating
6. Low thermal resistance RthJC
7. When choosing a package, consider the importance of RthJA.
8. The speed of the internal diode and the reverse recovery charge are not important as the internal diode rarely conducts current in the buck converter (only during forced down transitions of the output voltage).

The equations of power loss included the various losses into the HS-MOSFET are Equation (3.12):

$$P_{HScond} = I_{out}^2 R_{DSON\_HS} * D = 53.94 * 5m\Omega * (0.1) = 27mW \qquad (3.12)$$

The output capacitance is abasic parameter of MOSFETs. FOMOSS, related to the output board, maybe a implies of measuring the impact of energetic execution on different advances. In each cycle, the yield capacitance of the HS-MOSFET is charged when the HS-FET is turned off and canceled (scattered inside the channel) when the MOSFET is turned on. For the BSC050NE2LS, under sample conditions, the loss associated with the output capacitance is Equation (3.13):

$$P_{OSS\_HS} = 0.5 * Q_{OSS\_HS} * V_{IN} * f_{sw} = 0.5 * 6.4us * 29 * 5kHz = 0.464 \qquad (3.13)$$

For inductively restricted switching (rapid switching with an inductive plateau in the switching waveform), the switching loss is Equation (3.14):

$$P_{SW\_HS} = 0.5 * L_{Stray} I_o^2 f_{sw} \qquad (3.14)$$

For resistively constrained switching (slow switching with a gate charge plateau in the waveform), the switching loss is Equation (3.15):

$$P_{SW\_HS} = V_{in} I_{out} \frac{Q_{SW}}{V_{GS}} R_{Gate} f_{sw} \quad (3.15)$$

The switching charge must be provided to get the MOSFET from the threshold gate voltage to the end of the plateau (low VDS) in the gate charge characteristic. VGS is the control voltage, and reflects the entire resistance in the gate drive route (including MOSFET and driver). Because the control voltage fluctuates throughout the transition, this equation is only a first-order approximation. This is still an acceptable approximation for centered plateau stresses. Simulating the transition allows for more precise switching losses. The parasitic inductances of both MOSFETs may be simply taken into consideration in this case.

When switching quicker than the current changes between HS and LS-MOSFET in its switching circuit, the HS-MOSFET must have a low FOM to offer low RDSON. In addition, the driver must have a low enough drain and source impedance to quickly drive the MOSFET. The gate resistance of the MOSFET should likewise be low for the same reason (Haji and Genc 2018).

MOSFETs are available in a number of packages. The following factors should be considered while making a decision:

- Required RDSON determines the minimum packet size.
- Fast switching (limited by inductance) is only possible in packages with low inductive source feedback.
- Package resistance should be low to ensure good device FOM, it is very necessary for low RDSON MOSFETs.
- The thermal resistance of the cooling path packaging must be sufficiently low. If top side cooling is required, a case with a low R_{thJC} top should be selected. In some cases, thermal transient response is very important.

The needed thermal resistance to ambient R_{thJC} may be computed using the power loss of the MOSFET and the permissible temperature increase of its junction to ambient as in Equation (3.16):

$$R_{thJA} = \frac{T_J - T_A}{P_{MOSFET}} with: R_{thJA} = R_{thJC} + R_{thCA} \tag{3.16}$$

R_{thJC} is the thermal package resistance specified in the data sheet. This value is normally less than 5K/W for power MOSFETs. Under working circumstances, the MOSFET temperature rises by 50 K, allowing for a 5 W power loss in the MOSFET and a 5 K/W thermal resistance to the case, assuming the pcb is at ambient temperature. The thermal resistance casing to ambient is the defining and usually limiting factor (Baharudin *et al.* 2017).

3.2.4 Derivation of transfer function for a buck converter

The transfer function named as $\frac{\Delta V_{out}}{\Delta D}$ can be derived in two steps: firstly, considering the system is stable states, and then determining of amounts change for disturbances.

Consider the stable states of the system:

- The current of coil does not change into a period Equation (3.17):

$$I_L = \frac{V_{in} - V_o}{sL} D + \frac{-V_o}{sL}(1 - D) \tag{3.17}$$

- The amount capacitor charge does not change into a period Equation (3.18):

$$sCV_o = I_L - \frac{V_o}{R} \tag{3.18}$$

Determine amounts of change for an external disturbance, then, describing the transfer function: Equation (3.19), Equation (3.20), Equation (3.21) and Equation (3.22):

$$I_L = \frac{V_{in}-V_o}{sL}D + \frac{-V_o}{sL}(1-D) \quad (3.19)$$

$$sCV_o + \frac{V_o}{R} = I_L \quad (3.20)$$

Upon subsituting $I_L \rightarrow \underline{I_L} + \Delta i_L, V_o \rightarrow \underline{V_o} + \Delta v_o$

$$sL\Delta i_L = V_{in}\Delta D - \Delta v_o \quad (3.21)$$

$$sC\Delta v_o = \Delta i_L - \frac{\Delta v_o}{R} \quad (3.22)$$

Taking the previous equations to be a system of simultaneous equations and solving for $\frac{\Delta V_o}{\Delta D}$, we obtain the following from Equation (3.23):

$$\frac{\Delta V_o}{\Delta DV_{in}} = \frac{1/LC}{s^2+\frac{1}{RC}s+\frac{1}{LC}} \quad (3.23)$$

3.3 MPPT Techniques

A sub-section has 3 tracking techniques to drive the PV system to get the best operation point where the atmospheric conditions are changed during the time of system operating.

3.3.1 Algorithm of perturb and observe (P&O)

The classical algorithm of Perturb and Observe (Faranda and Leva 2008, Narendiran 2013, Sera *et al.* 2006) assumes an increase or decrease in the reference voltage Uref of the photovoltaic system in order to disturb the system at regular intervals and further compare the output power of the solar module at k and k-1 stages of operation. If, when the output voltage of the solar module changes on the k-th measurement interval, its power increases (transitions A2 → A1, B2 → B1 in Figure 3.4), then the control system continues to move the operating point of the solar module in this direction; otherwise, the sign of the reference voltage increment ΔV_ref changes, and the operating point of the solar module moves in the opposite direction. At each next stage of the disturbance, the algorithm presented in Figure 3.5 continues to work in the same way.

One of the main advantage when using this approach can be noted easily is the simplicity of the algorithm implementation.

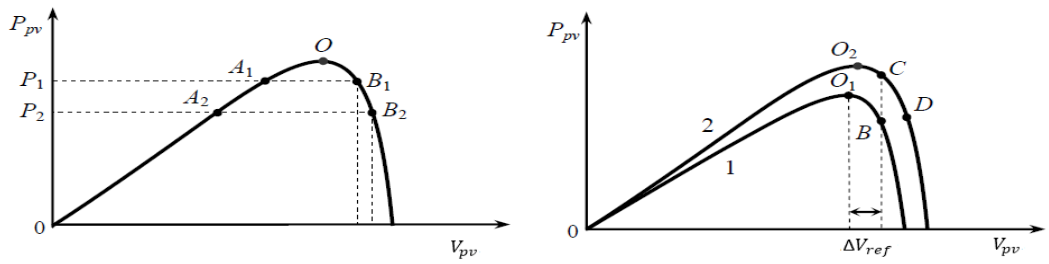

Figure 3.4 Movement of the solar module operating point in conditions of (a) constant and (b) variable solar radiation.

The parmeters $V_{pv}(k)$, $I_{pv}(k)$, $P_{pv}(k)$ in the chart Figure 3.5 are voltage, current and power of the solar module on the k interval of MPPT search; Uref (k) - PV reference voltage of the system that sets the voltage at the output of the solar module.

As noted above, the power regulation of the solar module is carried out using a step-up or step-down DC voltage converter. If we consider the output voltage of the converter unchanged, the voltage of the solar panel will change in accordance with the well-known equalities $V_{pv} = V_o(1-\gamma)$ for the boost converter and $V_{pv} = V_o/\gamma$ for the down converter, where Uout is the output voltage of the voltage converter, to the input of which voltage from the output of the solar module V_{pv}, γ is the relative duration of the open state of the power switch of the voltage converter. When the operating point moves from A2 to A1 (Figure 3.6), the solar module voltage V_{pv} increases (the control system receives a positive increment of ΔV_{ref}), which corresponds to a decrease in γ (the control system receives a negative increment of Δ γ). And, conversely, when the operating point moves to MPPT O from B2 to B1, the voltage of the solar module V_{pv} decreases (the control system receives a negative increment ΔV_{ref}), which corresponds to an increase in γ (the control system receives a positive increment of Δ γ).

In its simplest form, this algorithm tends to perform well as long as solar radiation does not change too quickly. These steady-state oscillations are highly dependent on the step size of the disturbance and the frequency of the disturbance. The disturbance frequency must be low enough for the PV system to reach steady state before the next disturbance. The size of the disturbance step should be sufficient so that the controller is not significantly influenced by interference when generating a new value of the output voltage (Elgendy *et al.* 2011, Femia *et al.* 2005).

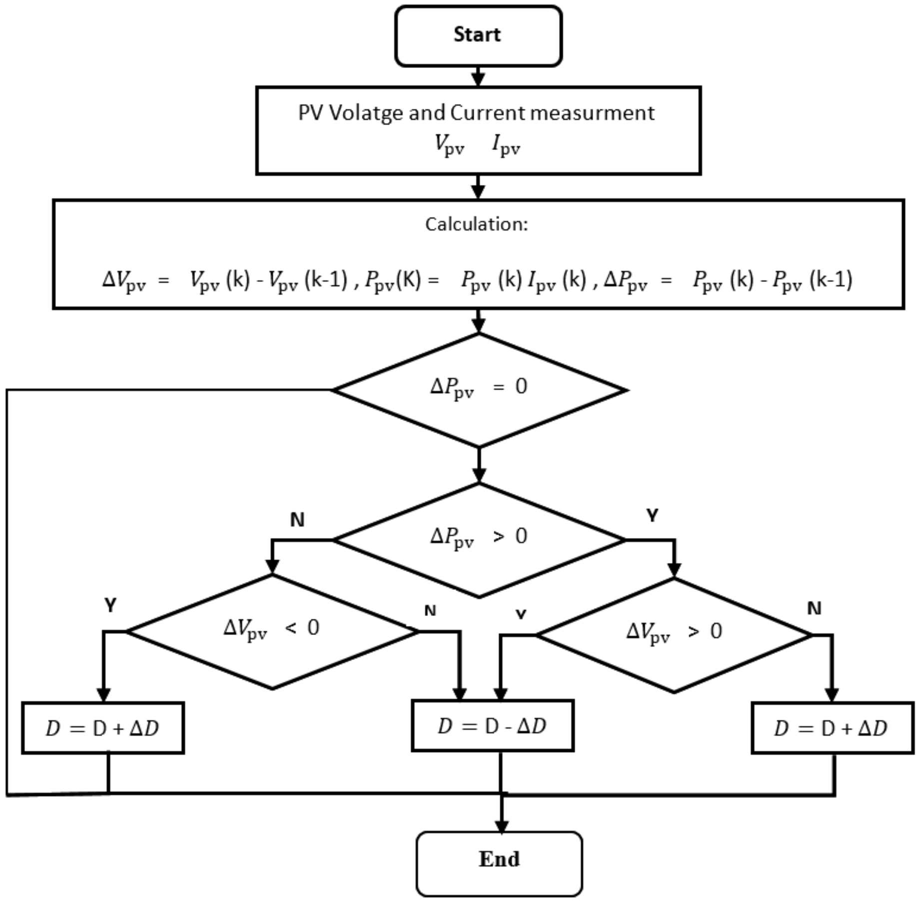

Figure 3.5 Block diagram of P&O algorithm

The disadvantage of the classic P&O algorithm is its low efficiency at low solar radiation (Selvan and Kumar 2015). For this cause, alternative solution has been suggested. For example, in (Dorofte *et al.* 2005) , the P&O algorithm is combined with a constant voltage (CV) algorithm to track MPPT with the highest efficiency at both cases low and high levels of solar radiation. The algorithm increases the duration of the open state of the power switch of the DC-voltage converter until the output voltage of the solar module is equal to approximately 76% of the open-circuit voltage, which is the starting point for the MPPT controller. The algorithm then calculates the output current of the solar module.

When the current exceeds the level corresponding to the minimum power of solar radiation, the algorithm uses the P&O method; if the current is lower, then the algorithm uses the CV method. The simulation results (Dorofte *et al.* 2005) show that the efficiency of solar energy extraction is from 95% to 99% in a wide range of solar radiation. (APPENDIX 1).

The P&O algorithm is prone to unstable behavior under conditions of rapid changes in the illumination level, since any change in the latter is perceived by the algorithm as a result of a change in the reference voltage at the previous stage. This can lead to slow or incorrect MPPT tracking. For example, a Figure 3.4, b explains the departure of the algorithm from the correct direction of the MPPT search. Let O1 be the starting point of the search. Assuming that the sign of the disturbance ΔV_{ref} is positive, the new operating point will be B. With constant illumination, the algorithm will detect a decrease in the power of the solar module and change the sign of the disturbance. However, if the illumination increases (transition from curve 1 to curve 2) at the k-th sampling interval, the new operating point will be point C, not B. The increase in solar module power will be perceived as a result of the disturbance, and the direction of the increment will remain. Therefore, the new operating point will be point D, which is clearly further from the true MPPT O2. If there is a steady rise in illumination, the operating point will continue to drift away from the true MPPT.

To solve this problem, various modifications of the P&O algorithm have been proposed. For example, in (Hsiao and Chen 2002), a three-point method is proposed that compares the power of a solar module at a test point with the power measured before and after the test point. In (Femia *et al.* 2005), to reduce fluctuations around MPPT and reduce the problem of rapidly changing solar radiation, it is shown how the parameters of the P&O algorithm (in particular, the sampling frequency of the current and voltage of the solar module) can be optimized for the dynamic behavior of a specific voltage converter.

In (Sera *et al.* 2006), a simple and effective solution to the problem of tracking MPPT in the wrong direction is proposed - the dP-P&O algorithm. In this algorithm, the power measurement is deconstructed to identify various sources of variation in the solar module power - as a result of disturbance or changes in solar radiation. The algorithm takes into account only the power changes caused by the actions of the MPPT controller as a result of the execution of its commands. The dP-P&O algorithm assumes an additional measurement of the power P_x of the solar module at a point corresponding to the middle of the sampling period T, as shown in Figure 3.6 (Ali *et al.* 2022).

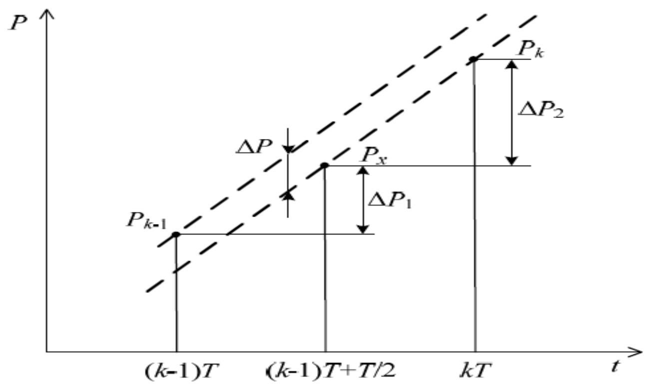

Figure 3.6 Illustration of calculating the power gain of the dP-P&O algorithm

The change in the power of the solar module ΔP2 is due to a change in only solar radiation, and the change in ΔP1 is due to the power caused by the disturbance from the MPPT controller and the change in solar radiation (Salman *et al.* 2018, Xuyang *et al.* 2017) . Assuming that the rate of change of solar radiation is constant within one iteration of the reference voltage (this corresponds to the same slope of the curves in Figure 3.6), the power increment due to the action of the MPPT controller could be calculated by the formula Equation (3.24):

$$\Delta P = \Delta P_1 - \Delta P_2 = (P_x - P_{k-1}) - (P_k - P_x) = 2P_x - P_k - P_{k-1} \quad (3.24)$$

In the dP-P&O algorithm, the calculation of the power increment $\Delta P_{pv=} P_{pv}(k) - P_{pv}(k - 1)$, inherent in the P&O algorithm in Figure 3.6, is replaced by the calculation of the power increment. The authors of (Biabani and Ahmed 2016, Sera *et al.* 2006) show that the dP-P&O method is able to prevent tracking in the wrong direction, inherent in the P&O algorithm during rapid changes in radiation, and is accompanied by a significant increase in tracking speed.

3.3.2 Incremental conductance (IC) algorithm

It is known that at the point of maximum cardinality the equality as follow Equation (3.25):

$$\frac{dP_{pv}}{dV_{pv}} = \frac{d(V_{pv}I_{pv})}{dV_{pv}} = I_{pv} + V_{pv}\frac{dI_{pv}}{dV_{pv}} = 0 \quad (3.25)$$

Which can be converted to the form Equation (3.26):

$$\frac{dI_{pv}}{dV_{pv}} + \frac{I_{pv}}{V_{pv}} = 0 \quad (3.26)$$

where I_{pv} and V_{pv} are the current and voltage of the solar module; $\frac{I_{pv}}{V_{pv}}$ - conductivity of the solar module; $\frac{dI_{pv}}{dV_{pv}}$ - incremental (increasing) conductivity. The fulfillment of condition (2) in the absence of a change in the solar module current (dI_{pv} = 0), caused by a change in the intensity of solar radiation, allows the control system to maintain the nominal voltage of the solar module found in this way without additional disturbance. The algorithm on the k-th operating interval begins with measuring the current values of the current $I_{pv}(k)$ and voltage $V_{pv}(k)$of the solar module. Then, using the corresponding values obtained in the k - 1 interval of operation, the increments of current ΔIpv and voltage ΔV_{pv} are calculated. The main one is to check the fulfillment of equality (2), according to the results of which the reference voltage V_{ref}, which sets the voltage at the output terminals of the solar module, will be corrected (Bendib *et al.* 2015) as in Equation (3.27):

$$\frac{dI_{pv}}{dV_{pv}} + \frac{I_{pv}}{V_{pv}} < 0 \quad (3.27)$$

The operating point on the P_{pv} (V_{pv}) plane is to the right of the MPPT, therefore, the reference voltage is corrected downward at Equation (3.28):

$$\frac{dI_{pv}}{dV_{pv}} + \frac{I_{pv}}{V_{pv}} > 0 \quad (3.28)$$

The operating point of the solar module is to the left of the MPPT, which requires an increase in the reference voltage to bring the output voltage V_{pv} closer to the nominal. A check for the equality $\Delta V_{pv} = 0$ is included in the algorithm to determine whether a control action is required in the form of a reference voltage correction, if the solar module has already worked in the MPPT at the previous stage. Here, the change in atmospheric conditions ($\Delta I_{pv} \neq 0$) in accordance with the I - V characteristic of the solar module will determine in which direction it is necessary to change the reference voltage V_{ref} (Singh *et al.* 2021).

It should be noted that condition (2) is rarely satisfied exactly due to the approximate calculations of dI_{pv} and dV_{pv} performed in the MPPT controller. Therefore, condition (2) of MPPT correspondence can be written as Equation (3.29):

$$\left|\frac{dI_{pv}}{dV_{pv}} + \frac{I_{pv}}{V_{pv}}\right| \leq \varepsilon \quad (3.29)$$

Figure 3.7 shows the flow chart of IC algorithm, in which the conditions are very clear.

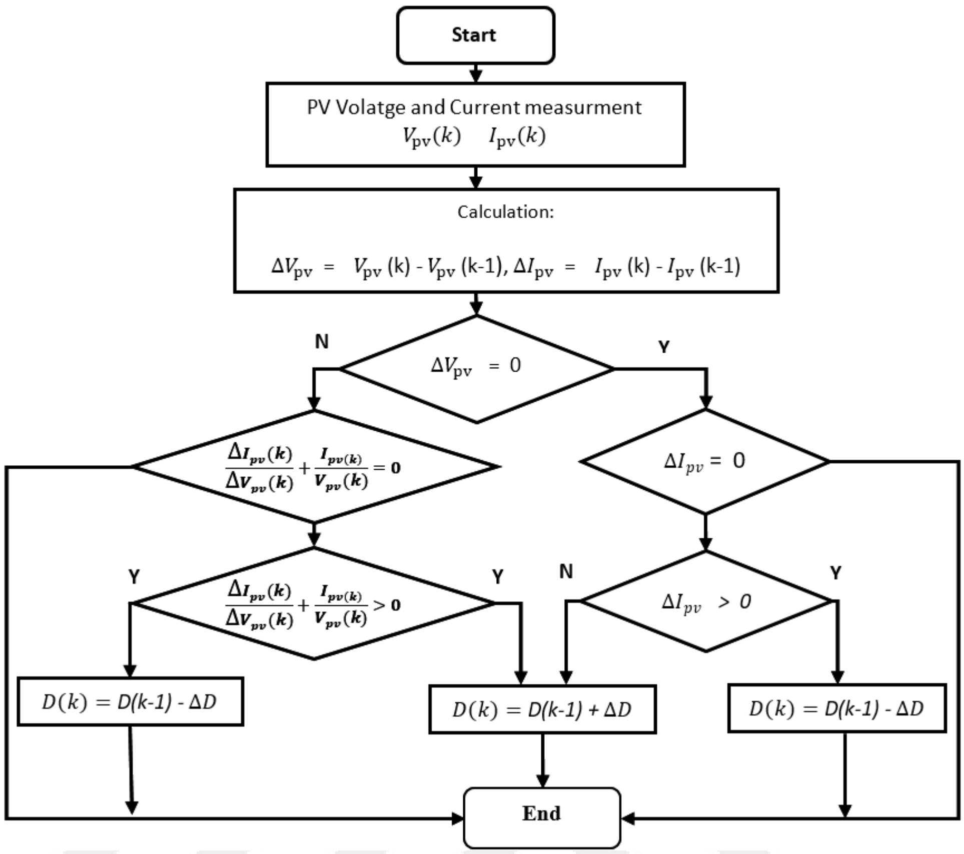

Figure 3.7 Flow chart of IC algorithm

The error value ε is determined from a compromise between finding the MPPT "exactly the same" and the prospect of fluctuations in the operating point around the MPPT. Thus, as in the P&O algorithm, to move the operating point along the volt-ampere characteristic of the solar module, a periodic perturbation of the control variable (in this case, the reference voltage) is required. However, continuous verification of condition (2) makes it possible to determine the position of the operating point relative to the MPPT. This, in turn, eliminates the initial adjustment of the reference voltage in the wrong direction, which occurs in the trial and error P&O algorithm.

The considered IC algorithm is characterized by a fast and correct system of response to changing operating conditions of the solar module, more accurate tracking of the MPPT and smaller fluctuations around it compared to the P&O algorithm (Esram and Chapman 2007, Salas *et al.* 2006). However, the IC algorithm has a disadvantage in that instability can occur due to the use of a differentiation operation in the algorithm. It should also be noted that at low levels of solar radiation, the differentiation operation is complex and tends to measure noise, so the results of the search for MPPT may be unsatisfactory (APPENDIX 2).

In general, the IC algorithm, when tracking a MPPT, uses a fixed iteration step size ΔV_{ref}, which is determined by the tracking accuracy and speed requirements. In (Lee *et al.* 2006), a modified IC algorithm with a variable step size was proposed. This approach automatically adjusts the step size when moving towards the solar module's operating point. When the operating point is considered to be far from the MPPT, the modified algorithm increases the step size to quickly approach the operating point to the MPPT, and vice versa, when the operating point is near the MPPT, the step size is reduced. By varying the step size, the accuracy and speed of the algorithm is increased. The small signal model confirms the stability of the system in almost all cases.

3.3.3 Fuzzy logic control technique

Renewable vitality sources have a wide run of applications for Fluffy Rationale Controllers (FLC). Over the past decade, FLC necessities have been expanded due to effortlessness (Ismail *et al.* 2010). FLC moreover bargains with loose input, which does not require an precise scientific show for the controller. FLC can easily tackle non-linearity conditions to get maximum power from PV modules. It is able to work in any weather conditions, with any changes in temperature or light level (Sharma and Jain 2015).

The operation algorithm of a calculator built on the basis of fuzzy logic consists of three stages; fuzzification, fuzzy inference and defuzzification (Patel and Agarwal 2008). For the fuzzy controller block, we define two variables at the input and one output variable. We will use the error ΔP/ΔV and the rate of its change as input variables Equation (3.30), Equation (3.31):

$$E(k) = \frac{P(k)-P(k-1)}{V(k)-V(k-1)} \tag{3.30}$$

$$\Delta E = E(k) - E(k-1) \tag{3.31}$$

Where P(k), P(k–1) is the current power of the solar cell and at the previous cycle, respectively, V(k), V(k–1) is the output voltage from the solar cell, current and at the previous cycle, respectively, E(k), E(k–1) – current error and on the previous cycle, respectively. The derivative ΔP/ΔV (Salas *et al.* 2006) makes it possible to determine on which side of the MPPT on the characteristic P(V) the system is currently located. Being in MPPT corresponds to ΔP/ΔV = 0 (Sera *et al.* 2006). The rate of increase of the error makes it possible to determine in which direction the operating point is shifted along the curve of PV power figure. The output variable is the duty cycle.

Each variable must be assigned membership functions, note Figure 3.8 below, which are error input variable in Figure 3.9, error slew rate input variable as in Figure 3.10 and duty cycle output variable as in Figure 3.11 (Abihana and Gonzalez 1993, Ansari 1998, Narendiran *et al.* 2016, Noman *et al.* 2012).

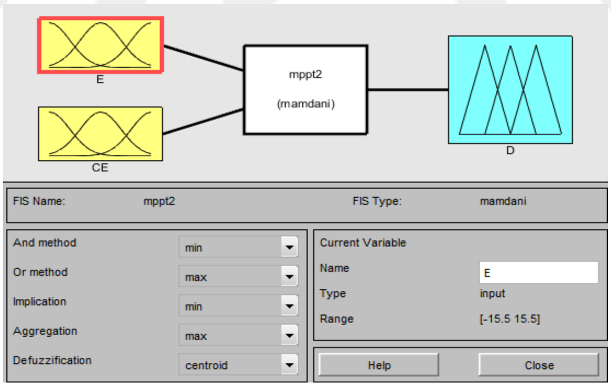

Figure 3.8 Membership function

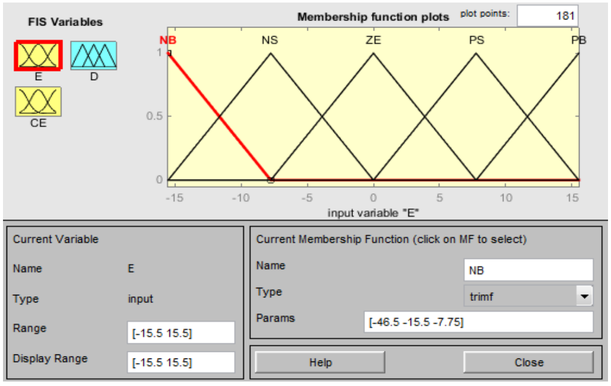

Figure 3.9 Input variable "error"

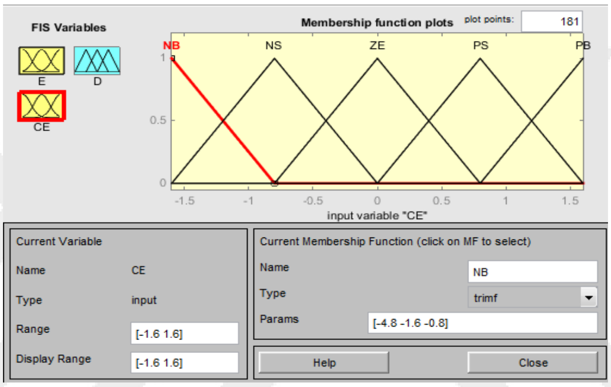

Figure 3.10 Input variable "error slew rate"

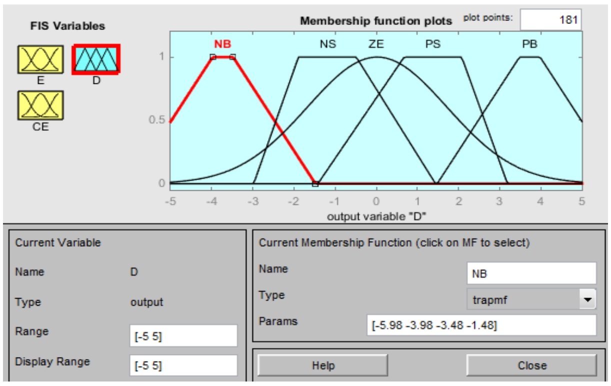

Figure 3.11 Duty cycle

Most often, 5 to 7 membership functions are enough: NB means large negative, NM means medium negative, NS means small negative, ZE means zero, PS means small positive, PM means medium positive and fiannly PB means large positive (Tajuddin *et al.* 2015, Tse *et al.* 2001). To describe the relationship between input and output quantities, you can use the base of production rules (Hsiao and Chen 2002, Mahalakshmi *et al*. 2014, Sivanandam *et al.* 2007). Table 3.2 shows these rules.

Table 3.2 Rules implemented in Fuzzy logic inference system

E / CE	NB	NS	ZE	PS	PB
NB	ZE	ZE	NS	PS	PB
NS	ZE	ZE	ZE	PS	PB
ZE	NB	NS	ZE	PS	PB
PS	NB	NS	ZE	ZE	ZE
PB	NB	NS	PS	ZE	ZE

In our case, one of the rules looks like: if E=NB and ΔE = NB then D = ZE (note Figure 3.12). This means: if the power received from the solar cell increases, it is necessary to increase the reference voltage by the change in the duty cycle until the TMM is reached (Dhanaraju *et al.* 2015, Doubabi *et al.* 2021, Noman *et al.* 2012) .

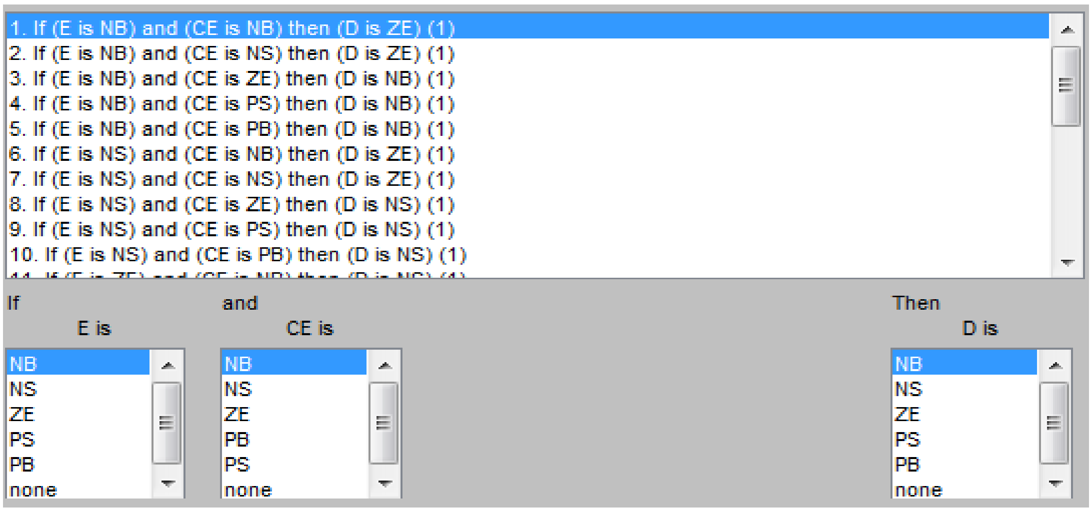

Figure 3.12 Fuzzy rules

3.4 DC-DC Converter for the Electrical Load Model

For modeling the storage battery, the method proposed by Olivier Tremblay and Louis-A was used. Dessaint (Tremblay *et al.* 2007, Tremblay and Dessaint 2009). The AB model is depended on the generalized Shepherd relation, it is given by the following Equation (3.32):

$$V_{batt} = E_0 - Ri - K\frac{Q}{Q-\int idt} + Ae^{-B\int idt} \tag{3.32}$$

Where $\int idt$ is representing the actual charge level of battery (measured by A·h); R is representing the internal resistance of battery (measured by Ohm); V_{batt} is the battery voltage (measured by V); i here is the battery current (measured by A); A, B are representing coefficients characterizing the magnitude of the voltage drop during the exponential discharge zone (V) and the reciprocal value of the battery capacity at the end of the exponential discharge zone (A·h)-1 and finally K is the polarization resistance (mesured by Ohm) (Sahin and Okumus 2011).

In the model which is used for the battery, the voltage value is defined by the values of the discharge current and the real level of charge of the SOC battery, that provides sufficiently accurate results for modeling the discharge and charge modes of battery of different types, including those used in energy systems with renewable energy sources: lead -acid, nickel-cadmium and lithium-ion (Jusoh *et al.* 2018).

The parameters of previous equation are determined by the battery discharge characteristic, set by the manufacturer. In the Simulink environment, this battery model is implemented as a standard battery block from the Sime Power Systems library, which was used in the research. The dialog box for entering the parameters of the AB model and the image of its functional block in the Simulink environment is shown in Figure 3.13 (Rebhi *et al*. 2013).

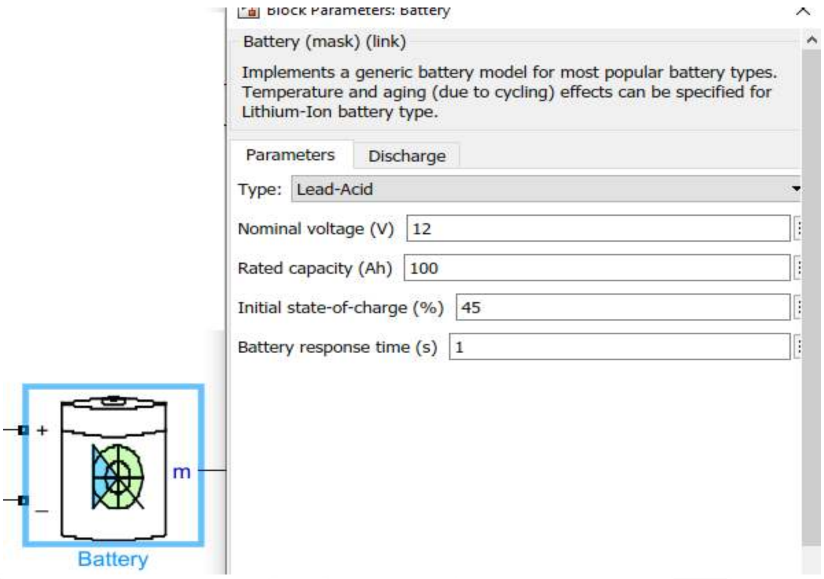

Figure 3.13 Dialog box for entering battery model parameters.

It should be noted that for the research tasks set, a battery model is required that adequately reflects only its dynamic characteristics, and the use of the model presented above is redundant. However, its use is justified by the fact that using the battery database built into Simulink, in this model it is very easy to change the type of batteries, their nominal voltage and residual capacity values. In this case, you do not need to take care of adjusting the values of the internal resistance of the battery, which are recalculated automatically. Figure 3.14 shows the nominal current discharge characteristic at 0.2C, this behavior could be represented as exponential function.

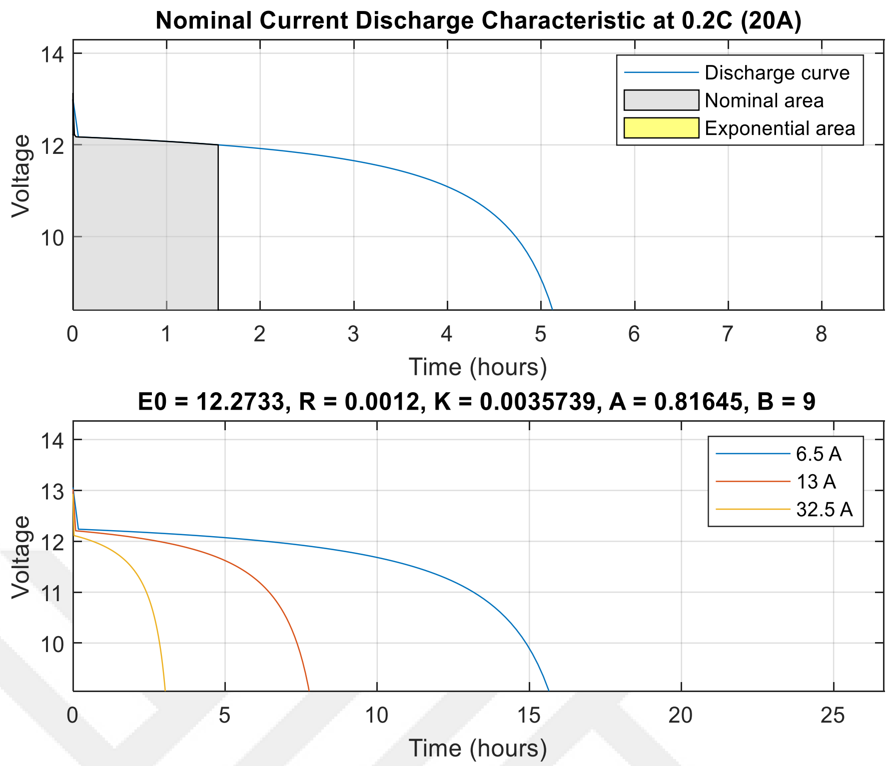

Figure 3.14 Nominal current discharge characteristic

4 SIMULATION OF PV SYSTEMS

4.1 Simulation of PV Model

After defining the mathematical relationships of the mathematical model of the solar cell in the second chapter, in this chapter a simulation model as presented in Figure 4.1 is built in the MATLAB environment based on the mathematical model and expressed in simulation blocks as in Figure 4.2 (Murtaza *et al.* 2013) (APPENDIX 3), (APPENDIX 4).

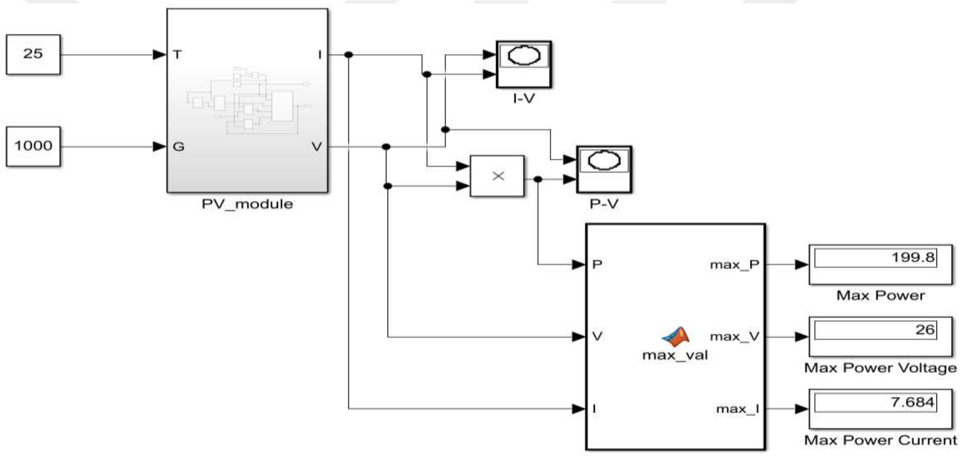

Figure 4.1 Simulation of PV max

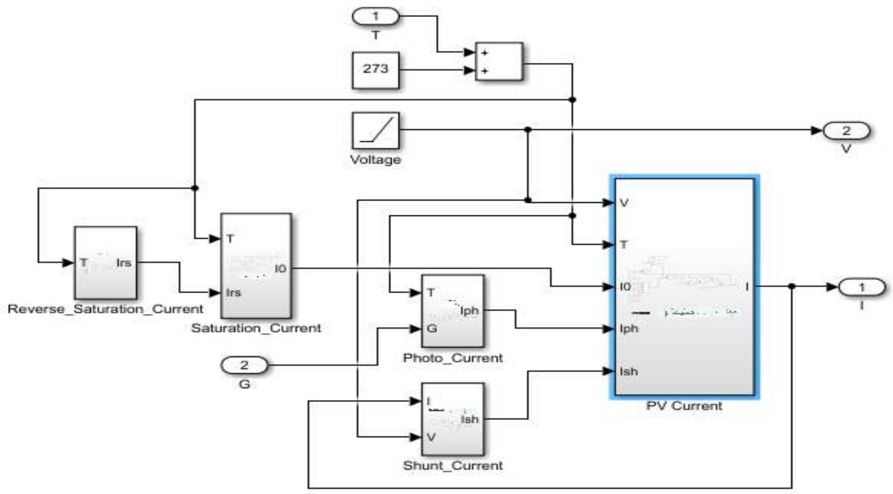

Figure 4.2 PV model in simulink

As shown in Figure 4.2, the PV model consists of the following subsystem:

- Reverse saturation current in Figure 4.3.
- Saturation current in Figure 4.4.
- Shunt current in Figure 4.5.
- Photo current in Figure 4.6.
- PV current in Figure 4.7, Figure 4.8, Figure 4.9

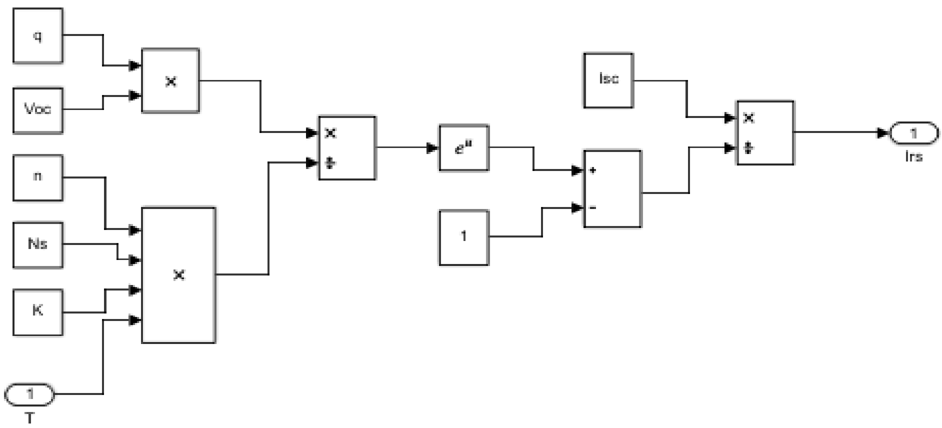

Figure 4.3 Reverse saturation current block

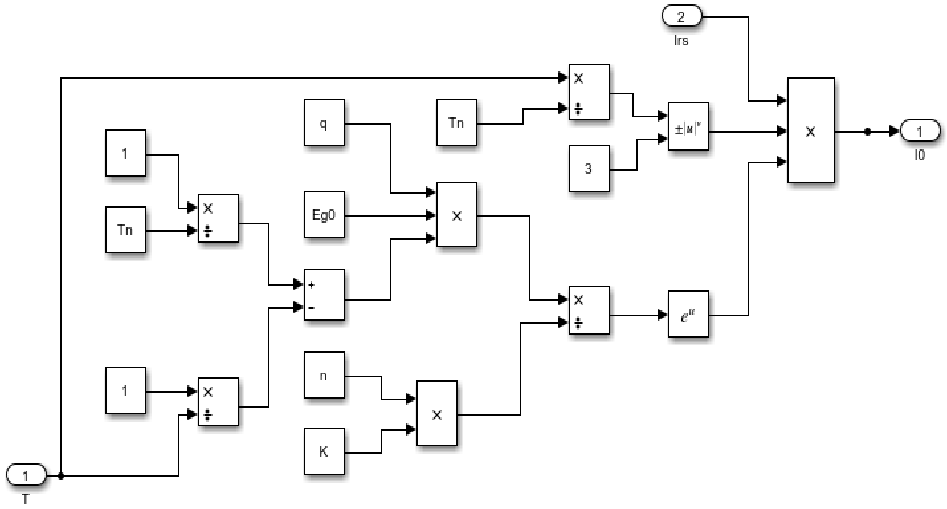

Figure 4.4 Saturation current block

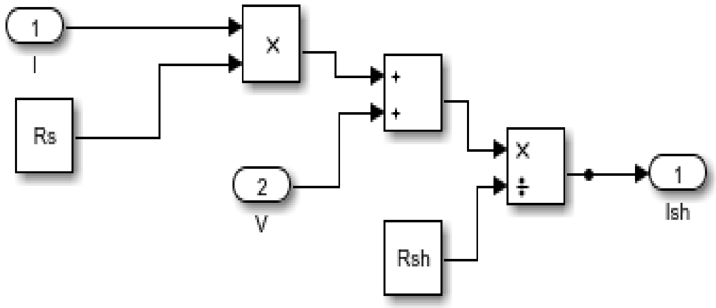

Figure 4.5 Shunt current block

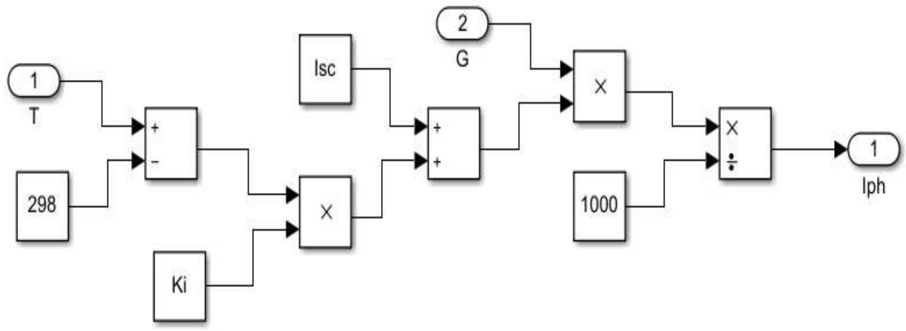

Figure 4.6 Photo current block

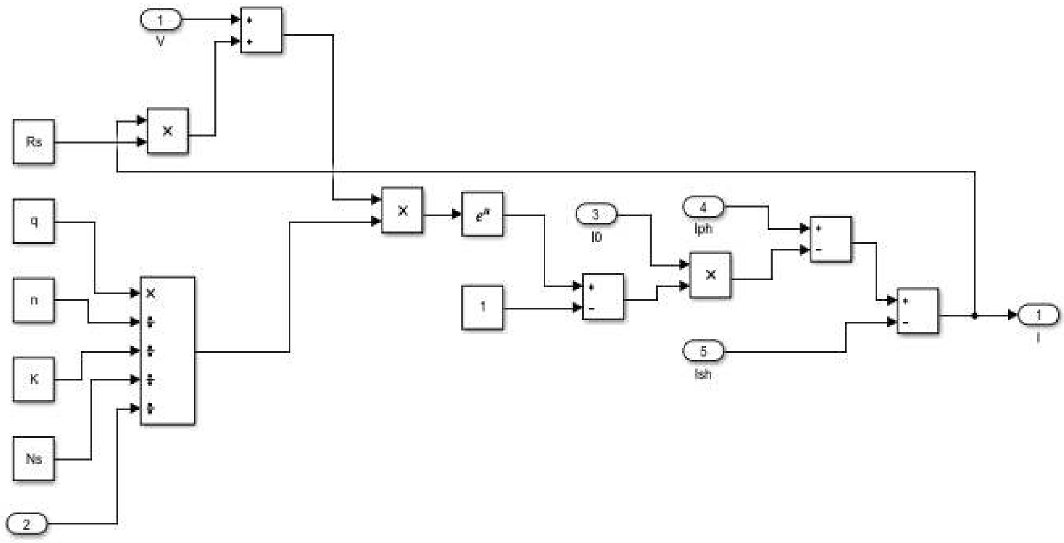

Figure 4.7 PV current

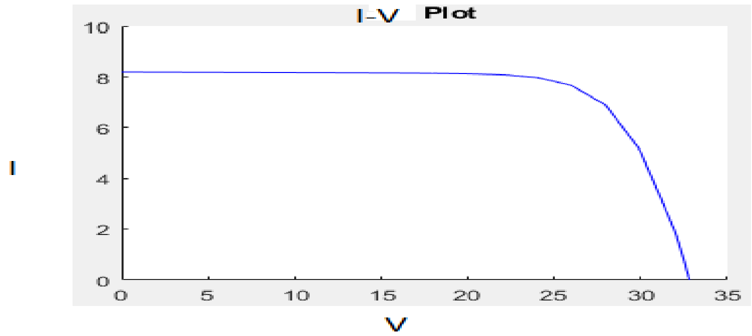

Figure 4.8 I_V characteristics of PV panel

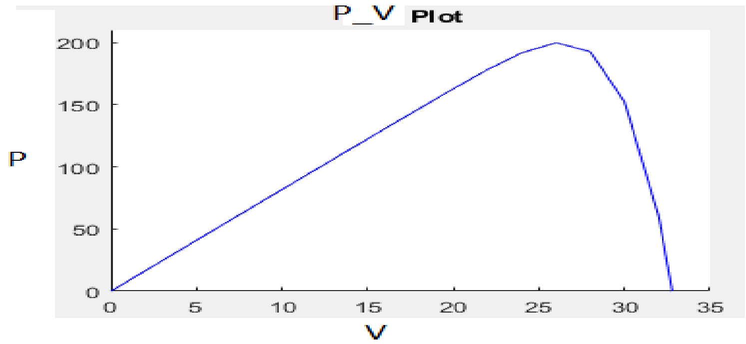

Figure 4.9 P_V characteristics of PV panel

In the project, the ready-made model was used in the Matlab environment 1STH-215-1Soltech which has the following characteristics as shown in Table 4.1 (POSHARP). Relations between the output current and voltage (volt-ampere characteristic), as well as between the power and voltage of the solar cell, are shown in Figure 4.10, Figure 4.11 respectively, 2 and 3 In the Table 4.1 shows the parameters of the considered solar panel.

Table 4.1 Solar panel parameters

1STH-215-P **1 series modules;1 parallel strings**	**Value**
Volatge st maximum power, V	29V
Cureent at maximum power, A	7.35A
Open circuit voltage, V	36.3V
Short circuit current, A	7.84A

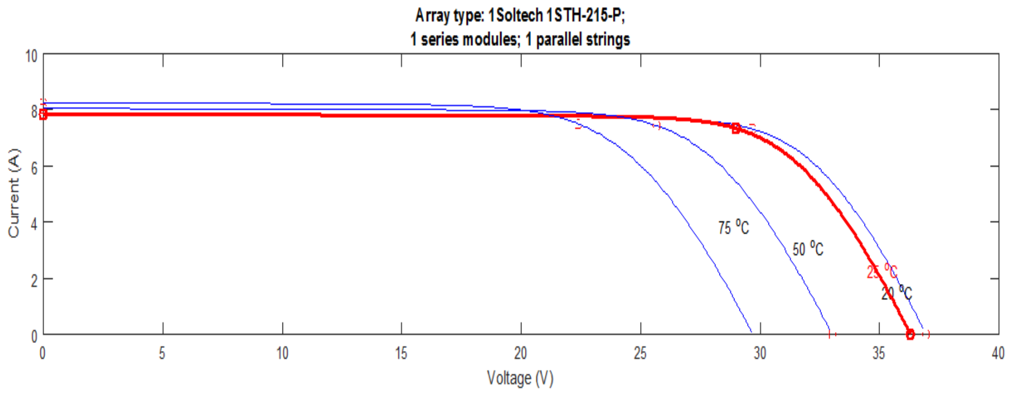

Figure 4.10 I-V solar cell characters

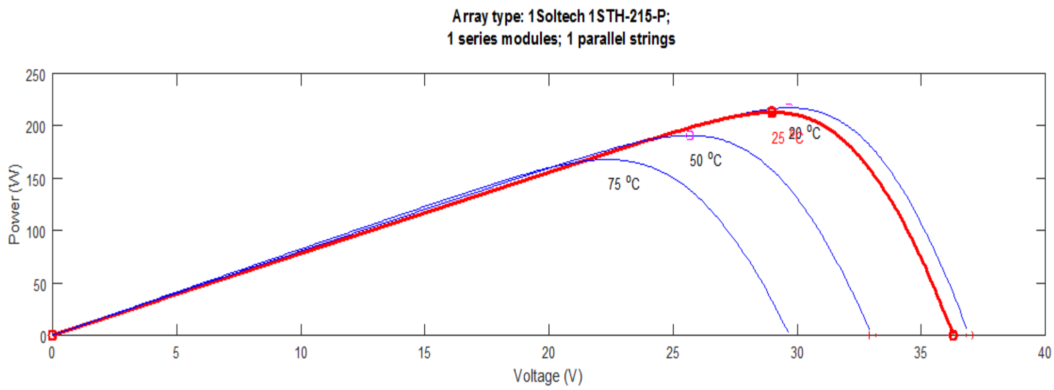

Figure 4.11 P-V solar cell characters

4.2 Simulation of DC-DC Buck Converter

For the value of the design in this project according to Table 3.1, the transfer function could be written as Equation (4.1):

$$\frac{\Delta V_o}{V_{in}} = \frac{\Delta D/LC}{s^2+\frac{1}{RC}s+\frac{1}{LC}} = \frac{2.32}{2.791*10^{-7}s^2+s+1} \tag{4.1}$$

As presented in Figure 4.12, the open-loop step response are given. It is obvious from the figure that the transient response of the buck converter is stable (no over shoot, settling time = 3.91sec).

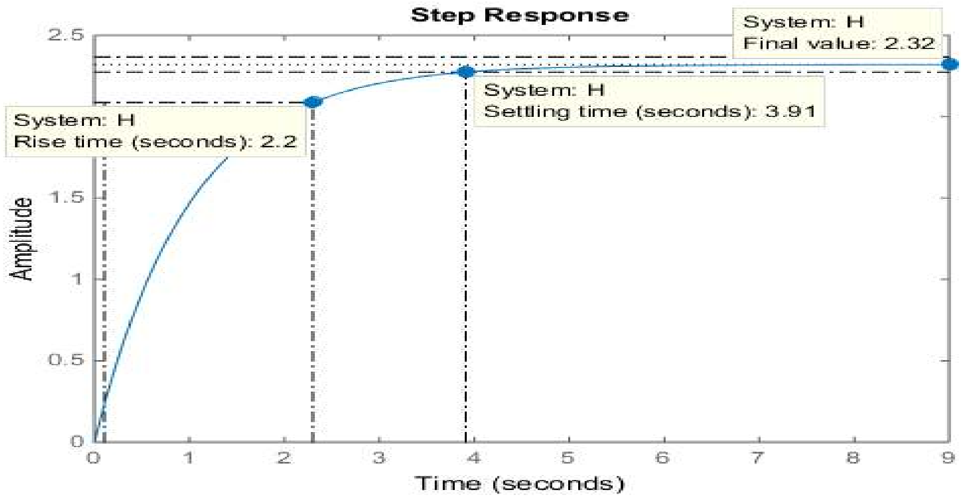

Figure 4.12 Buck converter step response

Figure 4.13 shows the bode plot of the buck converter, the phase margin is 116 degree, and gain margin infinity. The system is stable in closed loop.

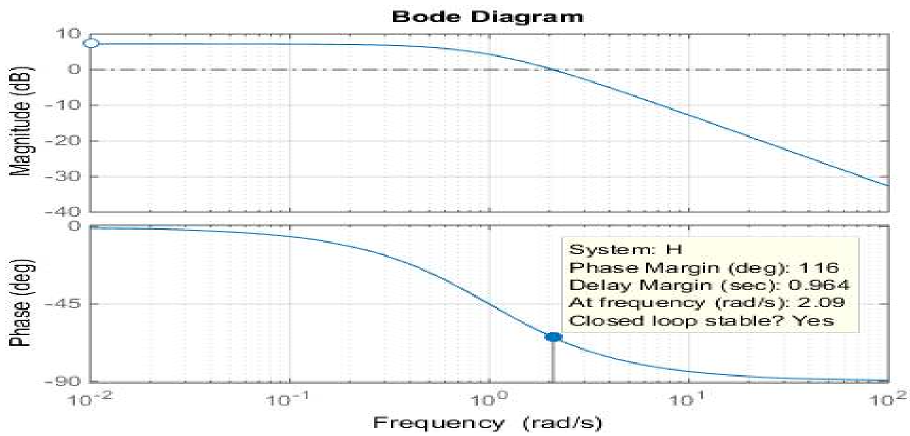

Figure 4.13 Buck converter bode plot

4.3 Simulation of PV System without MPPT Techniques

The system model in Figure 4.14 consists of the following subsystems :

- Irradiation blocks
- Temperature block
- PV block
- DC-DC buck converter
- Battery
- Switching signal blocks
- Scopes
- Results block (sub-system)

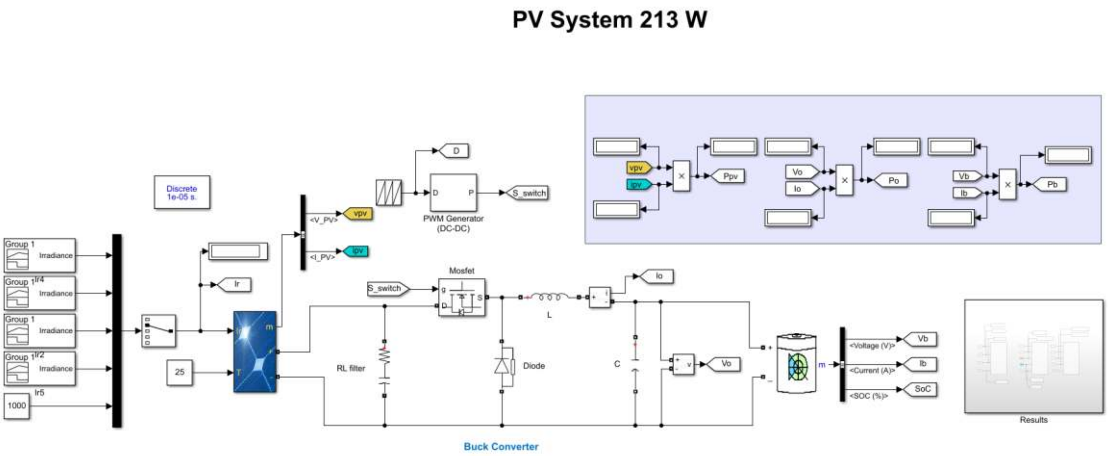

Figure 4.14 PV system without MPPT algorithm

The values and details of the circuit elements used in the circuit have presented in Figure 4.15, Figure 4.16, Figure 4.17, Figure 4.18 and Figure 4.19 to show the internal parmeters for each of the RL filter, the MOSFET, the diode, the inductor and the capacitor respectively.

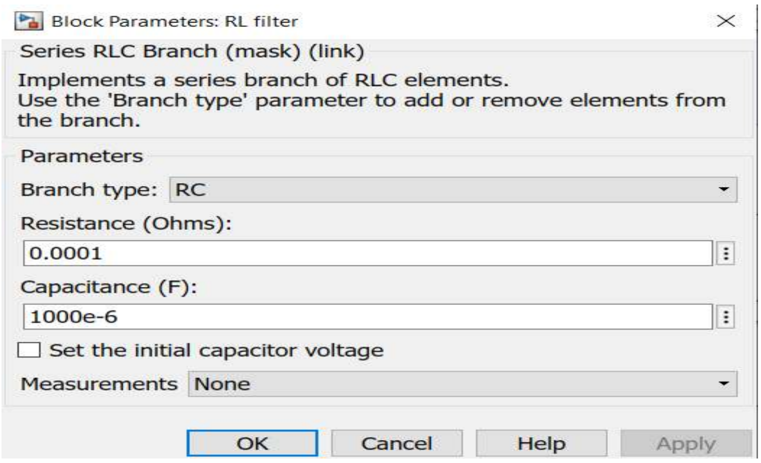

Figure 4.15 Window of the RL filter

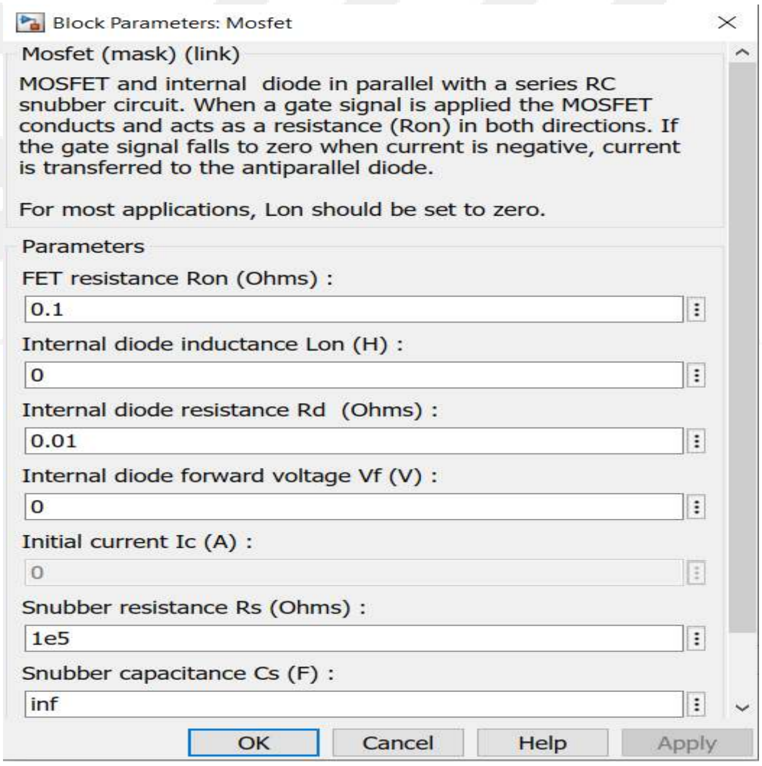

Figure 4.16 Window of the MOSFET

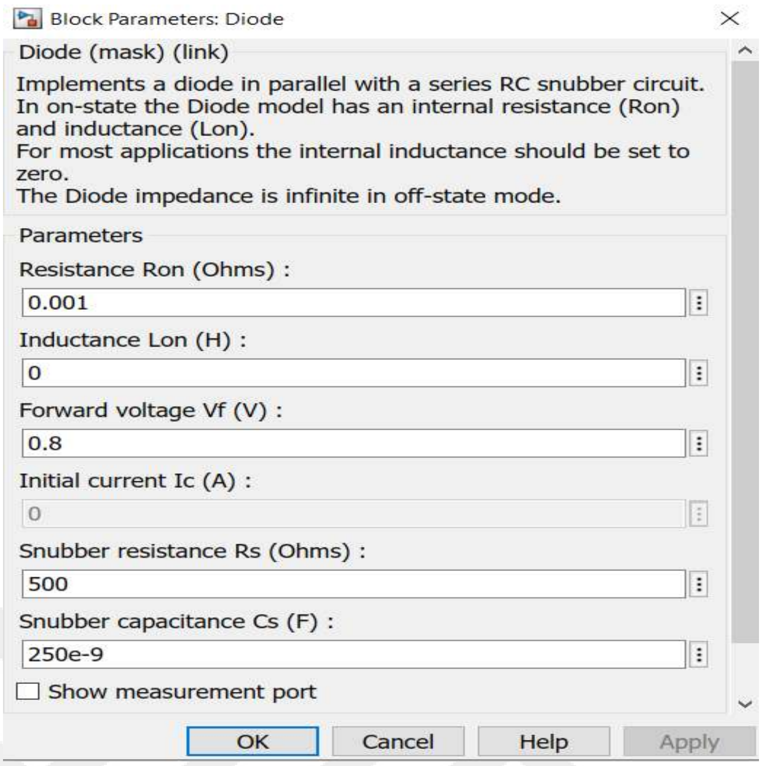

Figure 4.17 Window of the diode

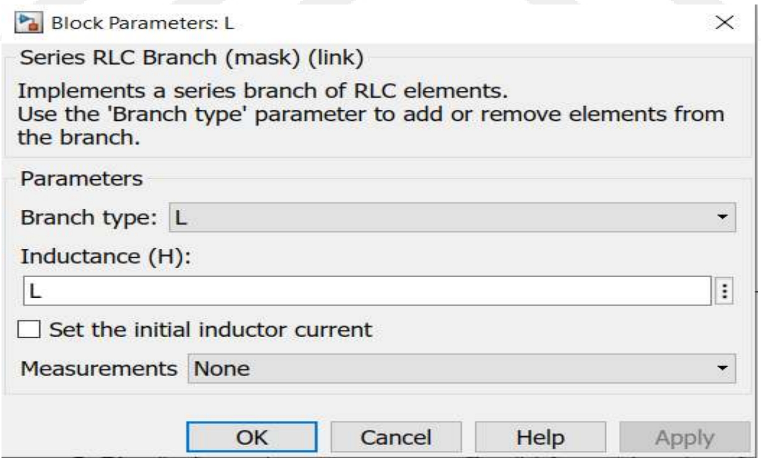

Figure 4.18 Window of the inductor

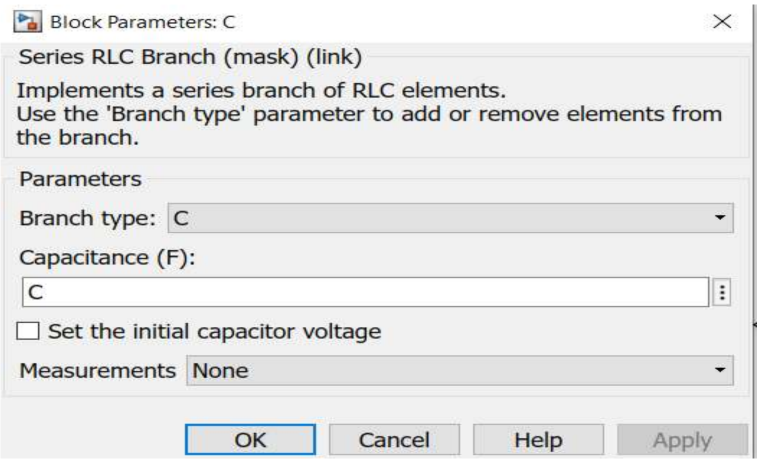

Figure 4.19 Window of the capacitor

The control signal (controller output) is compared with sawtooth signal as presentred in Figure 4.20 to make the pulse width modulation as in Figure 4.21 which drive the transistor in the DC-DC buck converter. Since there is no MPPT controller used in the current system, only sawtooth signal has used to make the pulse with modulation as shown in Figure 4.22.

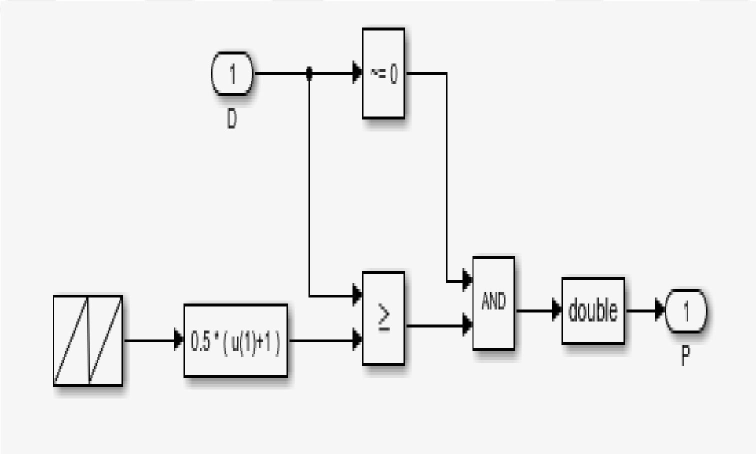

Figure 4.20 PWM generator

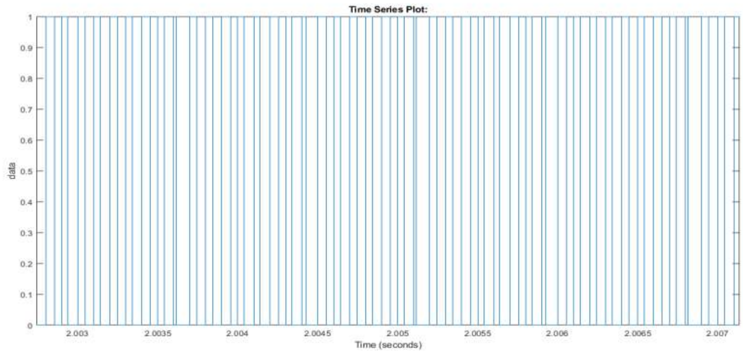

Figure 4.21 PWM control signal

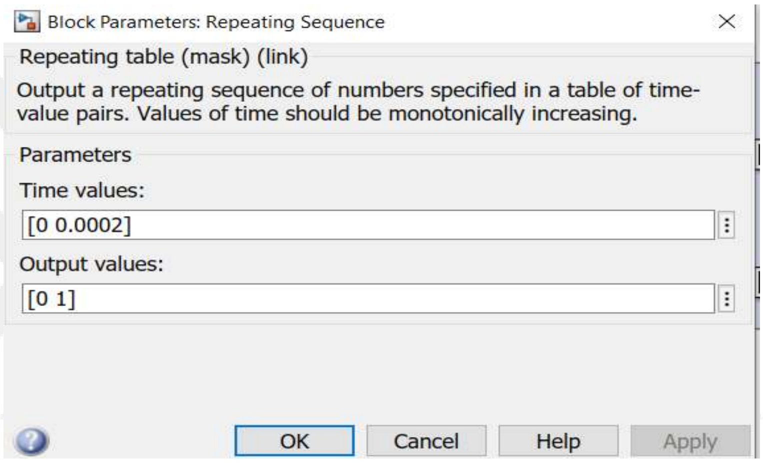

Figure 4.22 Window of the sawtooth signal

When the system has been operating, some of results have observed, Figure 4.23 showed the instability of the power drawn from the solar cell, and vibrations are observed around the value (160W), which is less than the maximum value that can be drawn. The voltage value as presented in Figure 4.24 also vibrates next to the value (21V) which is less than the maximum value. While the current as shown in Figure 4.25 reaches a maximum value with a rise time of 5 milliseconds and stabilizes in a time of 10 milliseconds with a static error of 200 milliamps.

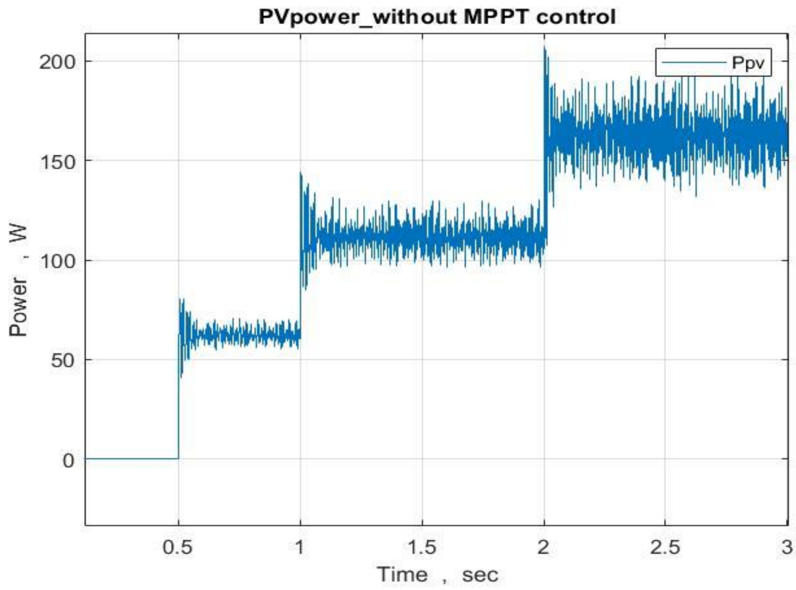

Figure 4.23 PV power without MPPT algorithm

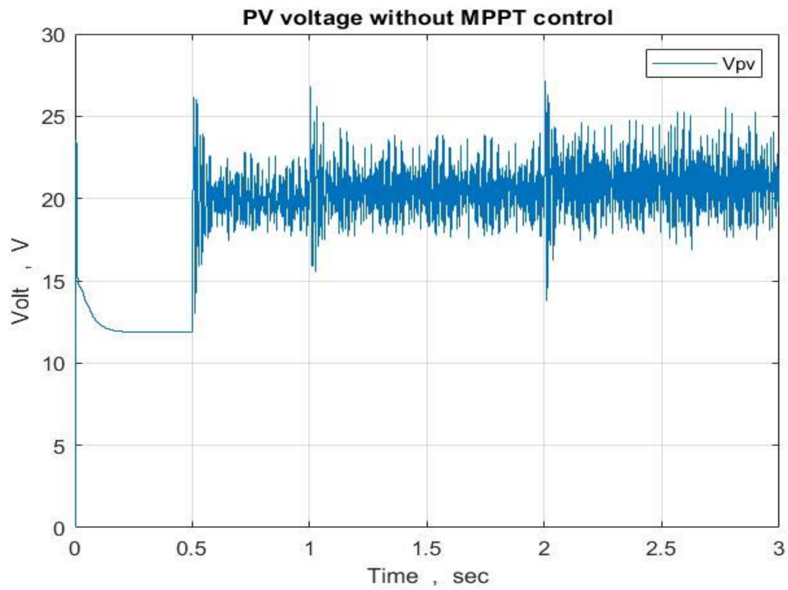

Figure 4.24 PV voltage without MPPT algorithm

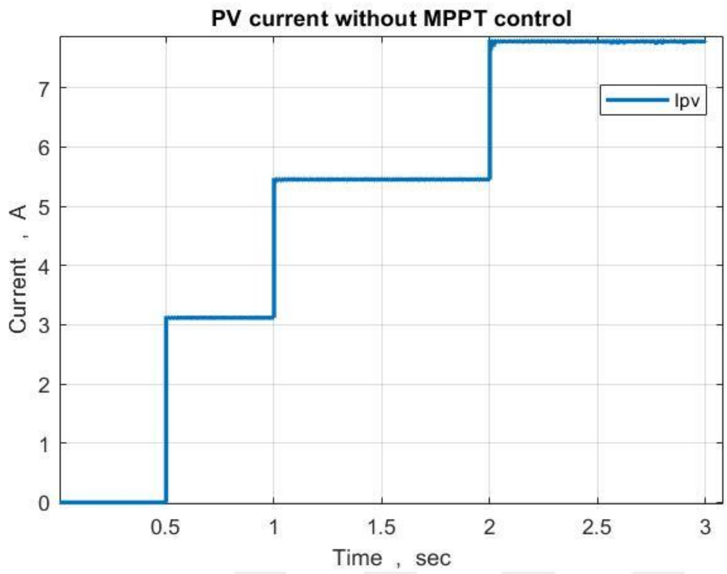

Figure 4.25 PV current without MPPT algorithm

4.4 Simulation of PV Sysytem Based MPPT Techniques

4.4.1 Uncontrolled battery

In this section, the result of PV parameters would be presented with MPPT techniques for the same irradiation vaules as presented in Figure 4.26.

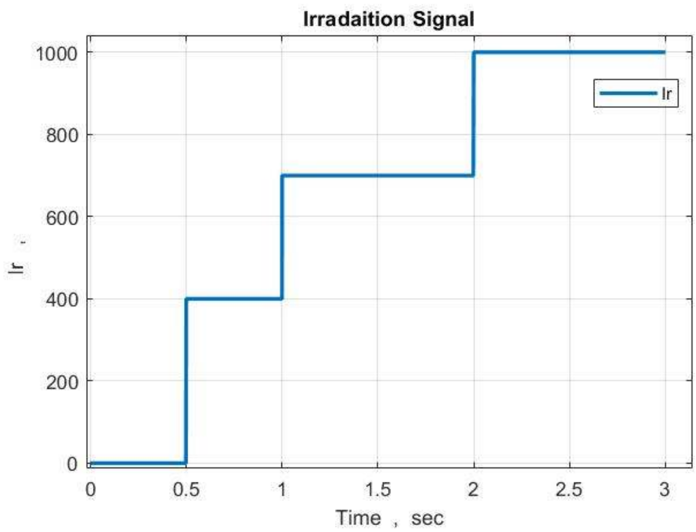

Figure 4.26 Irradiation signal

The system model in Figure 4.27 consists of the following subsystems (Sharma and Jain 2014):

- Irradiation block
- PV block
- DC-DC buck converter
- Battery
- Controller block
- Scopes

Where controller block changes according the MPPT algorithms. APPENDIX 1 and APPENDIX 2 show the algoritms of P&O and IC respectively, while Figure 4.28 presents the design of FLC sub-system.

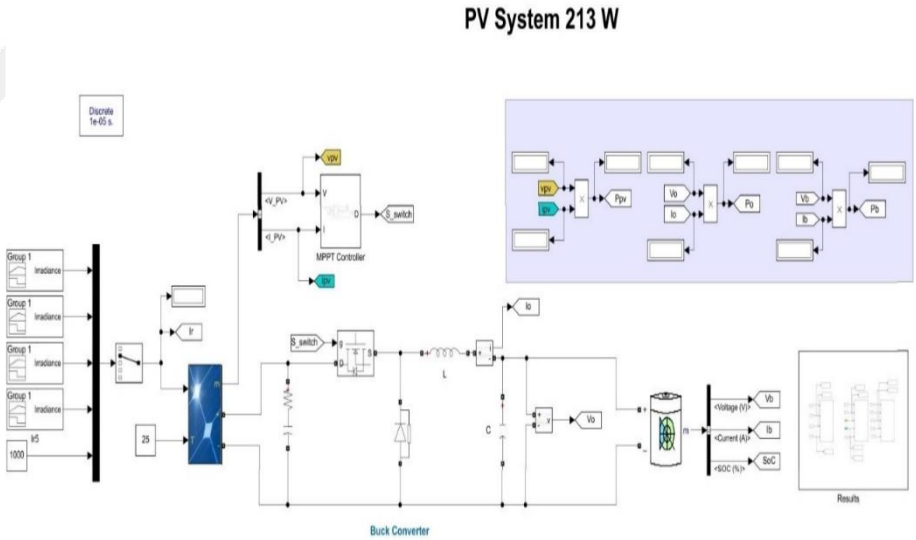

Figure 4.27 PV system based MPPT control techniques

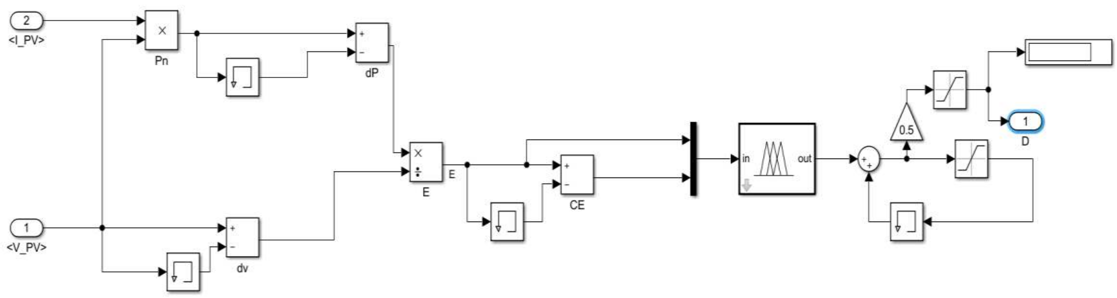

Figure 4.28 FLC sub-system

4.4.1.1 Simulation of perturb and observe (P&O) algorithm

Figure 4.29 shows the value of the power extracted from the solar cell, as it appears from the curve that the stability time of the power value on the final value is approximately 14 milliseconds, then a vibration next to the final value with an amplitude of 1 watt with a static error less than 4%.

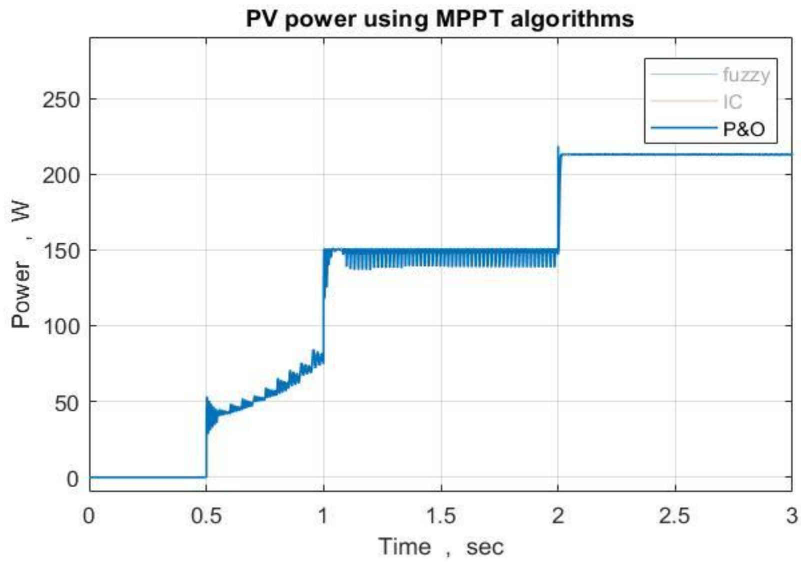

Figure 4.29 PV power using P&O algorithm

Figure 4.30 shows the value of the solar cell voltage, as it appears from the figure that a value greater than the maximum value that can be withdrawn from the solar cell is withdrawn, but for a short period of less than two seconds, then the voltage value vibrates next to the final (maximum) value, this large value causes damage to the solar cell with a large number of working hours. It is clearly noted that system is unstable with a low irradiation value.

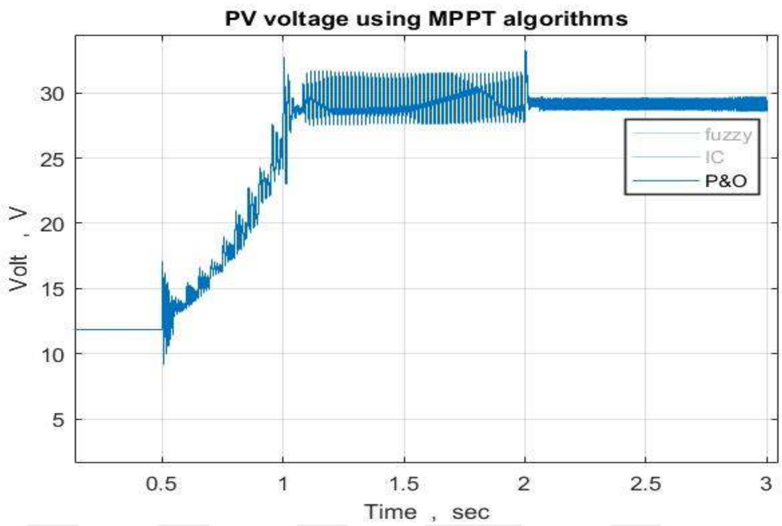

Figure 4.30 PV voltage using P&O algorithm

Figure 4.31 shows the value of the current from the solar cell, as the figure shows a short response time of 10 milliseconds and a static line of less than 200 milliamps.

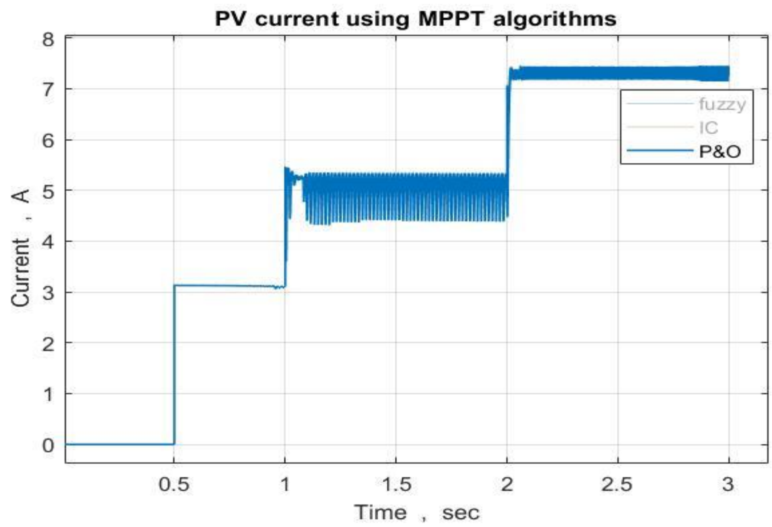

Figure 4.31 PV current using P&O algorithm

4.4.1.2 Simulation of incremntal conductance (IC) algorithm

Figure 4.32 shows the value of the power extracted from the solar cell, as it appears from the figure that the stability time of the power value on the final value is approximately 5 milliseconds, then a vibration next to the final value with an amplitude of 1 watt with a static error less than 3%.

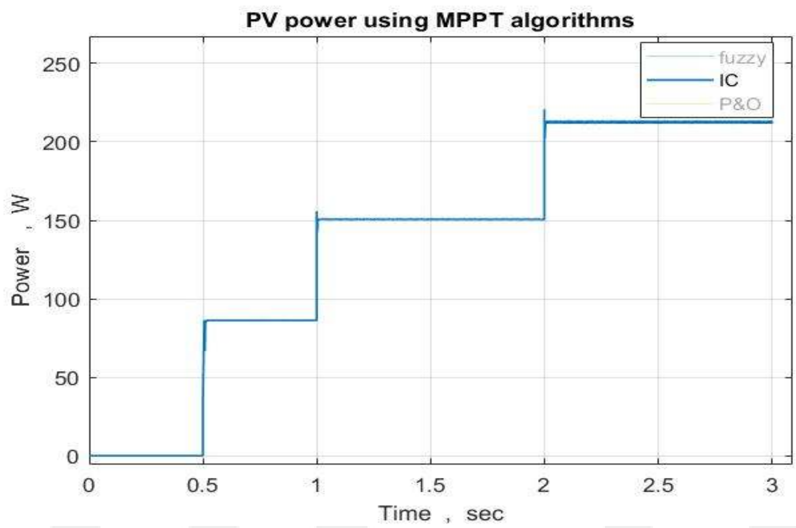

Figure 4.32 PV power using IC algorithm

Figure 4.33 shows the value of the solar cell voltage, as it appears from the figure that the voltage value vibrates next to the final (maximum) value with an amplitude less than a volt about 0.6 volt. The static error is less than one volt.

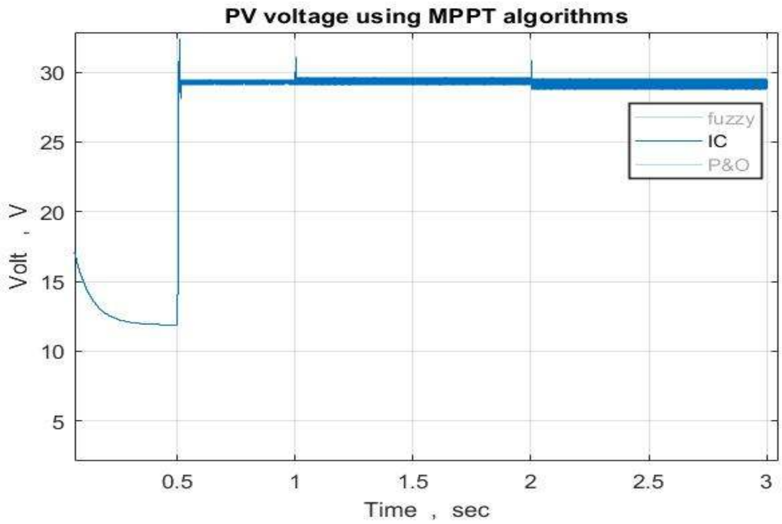

Figure 4.33 PV voltage using IC algorithm

Figure 4.34 presents the value of the current from the solar cell, as the figure shows a short response time of 30 milliseconds and a static line of less than 200 milliamps.

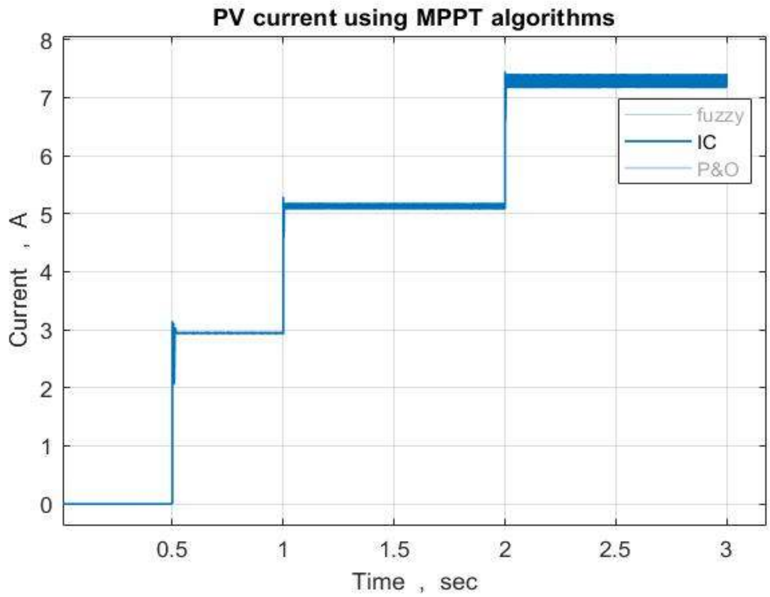

Figure 4.34 PV current using IC algorithm

4.4.1.3 Simulation of fuzzy logic control (FLC) technique

Figure 4.35 shows the value of the power extracted from the solar cell, as it appears from the figure that the stability time of the power value on the final value is approximately 5 milliseconds, then a vibration next to the final value with an amplitude of 1 watt with a static error less than 2%.

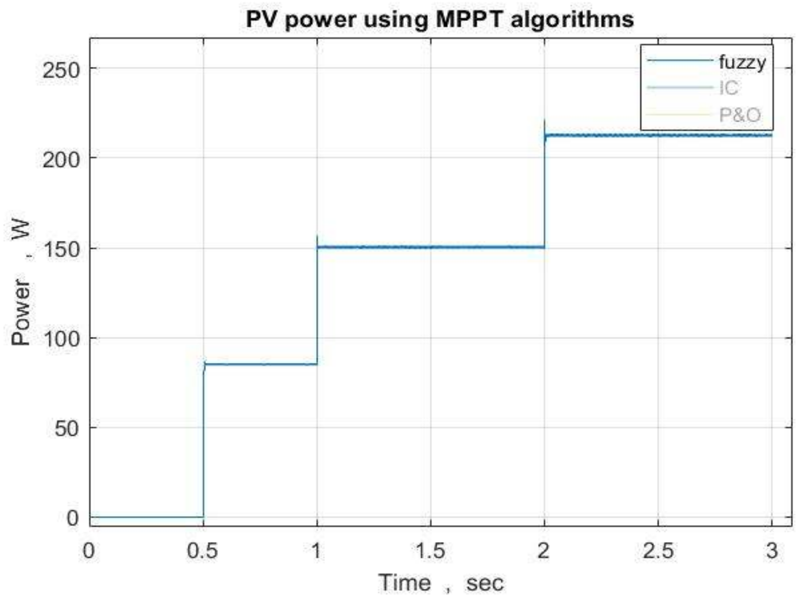

Figure 4.35 PV power using fuzzy algorithm

Figure 4.36 shows the value of the solar cell voltage, as it appears from the figure that the rise time is 7ms, then the voltage value vibrates next to the final (maximum) value with an amplitude less than a 0.6 volt and. The static error is approximately equal to 0.5 volt.

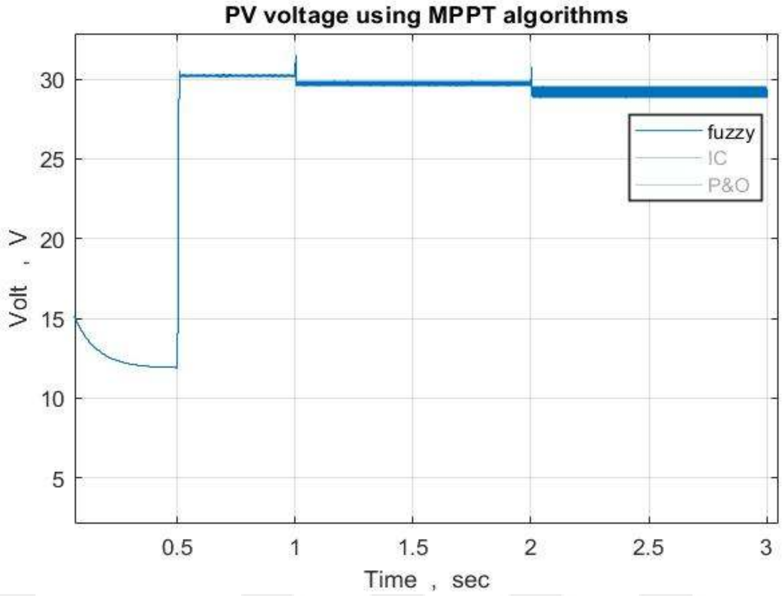

Figure 4.36 PV voltage using fuzzy algorithm

Figure 4.37 shows the value of the current from the solar cell, as the figure shows a short response time of 7 milliseconds and a static line of less than 200 milliamps, while Figure 4.38 shows the battery charge voltage.

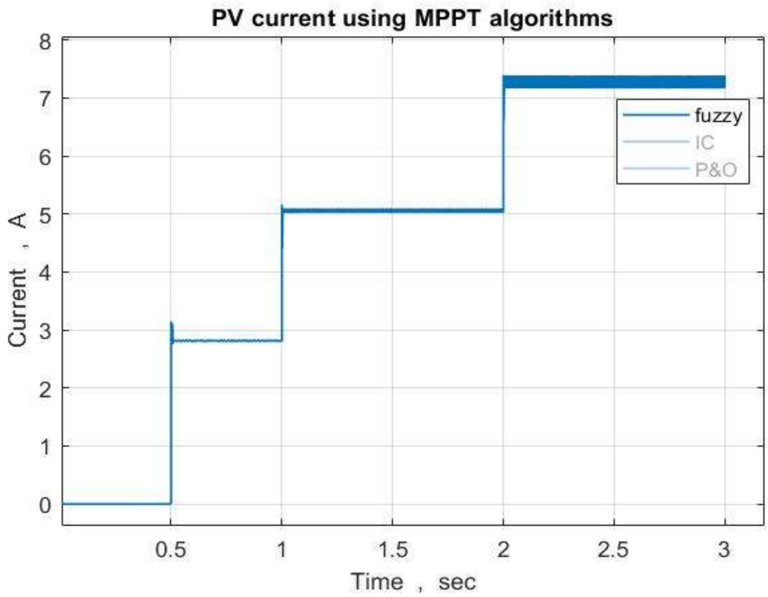

Figure 4.37 PV current using fuzzy algorithm

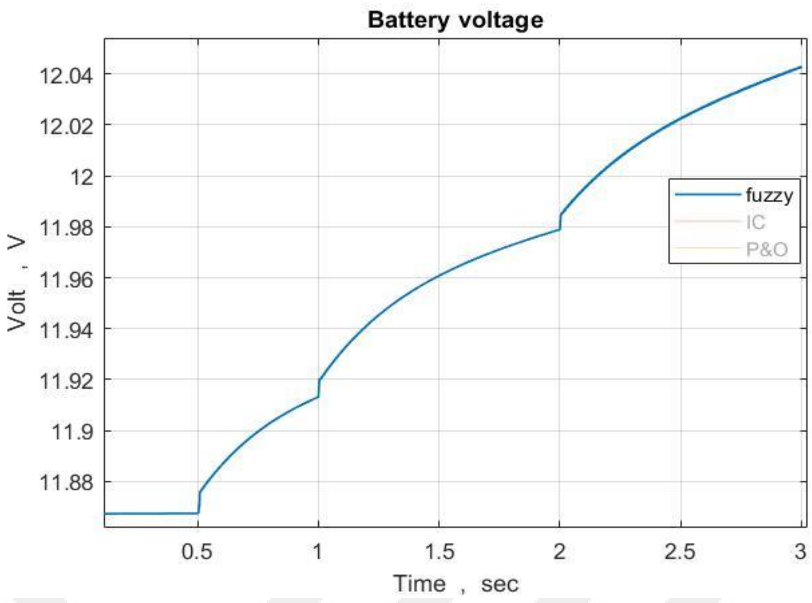

Figure 4.38 Battery charge voltage using fuzzy algorithm

4.4.2 Controlled battery

In this case study, Our PV system consists of a PV panel, DC-DC converter, MPPT controller, load, PI controller in addition to the sub-system of battery charge as shown in Figure 4.39, while Figure 4.40 prsents the bidirectional charge sub-system.

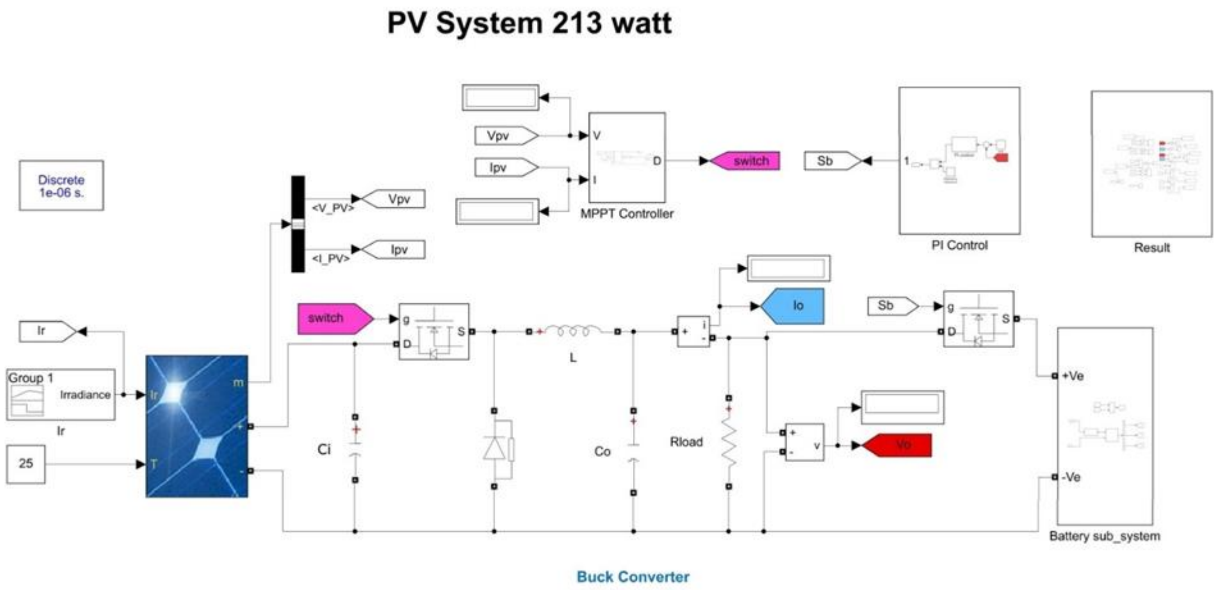

Figure 4.39 PV system in Simulation.

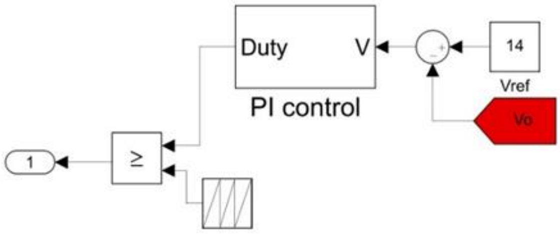

Figure 4.40 Bidirectional charge sub-system.

A test signal (Figure 4.41) that used for operating the system represents the irradiation, it has four varying stages where the values of irradiation change from 1000 to 700 w/m^2 at the period t=2 to 3 sec, then to 500 w/m^2 during the period 3-4 sec, and eventually return to 1000 w/m^2 during the period 3-4 sec. The purpose of that is to monitor the performance of the system, particularly during the transition period as well as comparison among the systems that used different three MPPT techniques P&O, IC and FLC. Figure 4.42, Figure 4.43 and Figure 4.44 are for the PV signals showing the power, current, and voltage of PV panel. Figure 4.45, Figure 4.46, and Figure 4.47 are for the output signals of systems, while Figure 4.48 and Figure 4.49 are for the battery current and voltage respectively. Finally, Figure 4.50 showed the charging signals for all the used techniques.

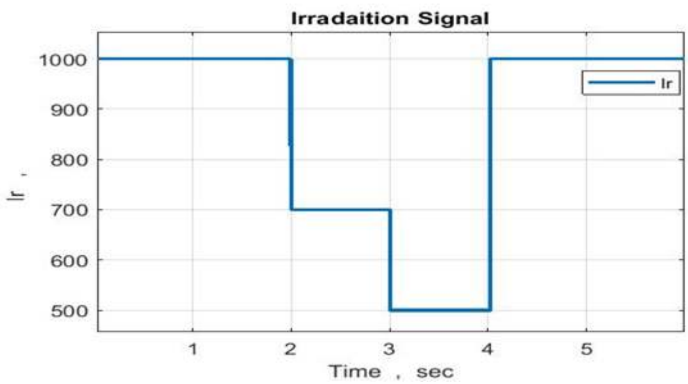

Figure 4.41 Irradiation signal.

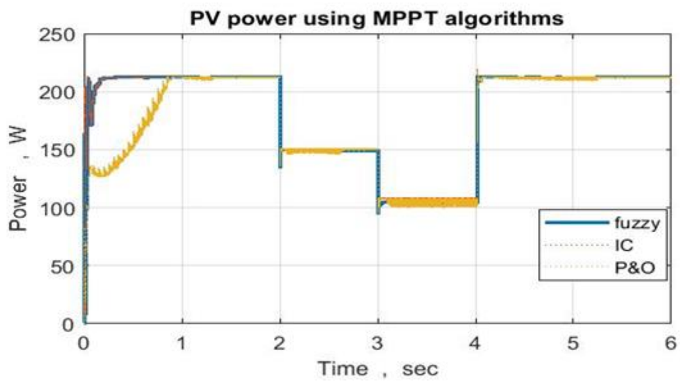

Figure 4.42 Power of PV panel.

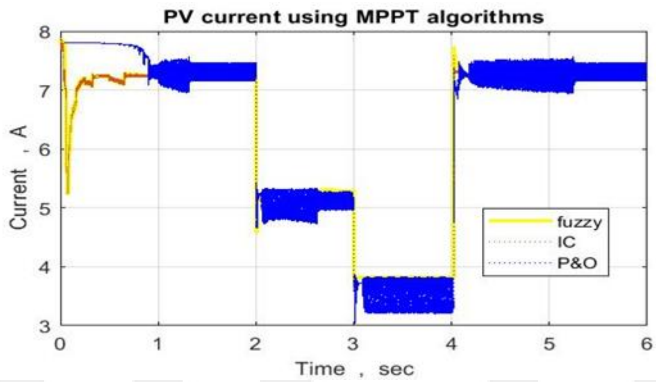

Figure 4.43 Current of PV panel.

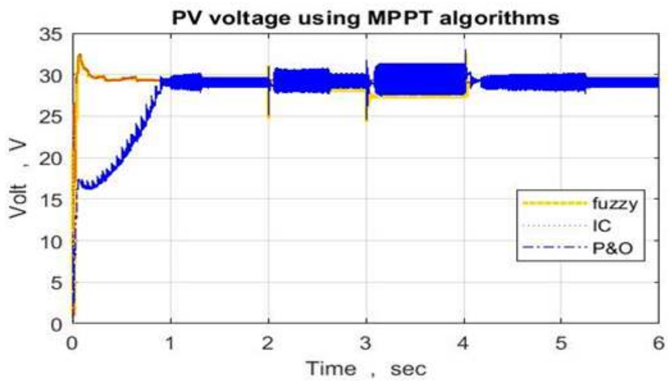

Figure 4.44 Voltage of PV panel.

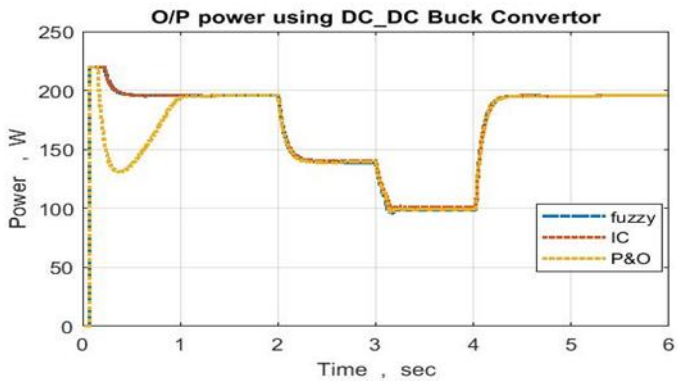

Figure 4.45 System output power.

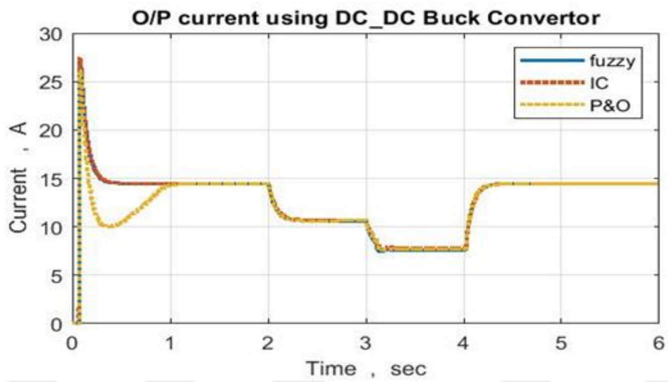

Figure 4.46 System output current.

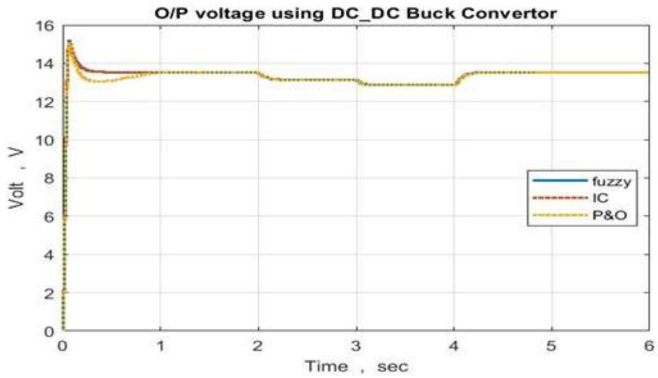

Figure 4.47 System output voltage.

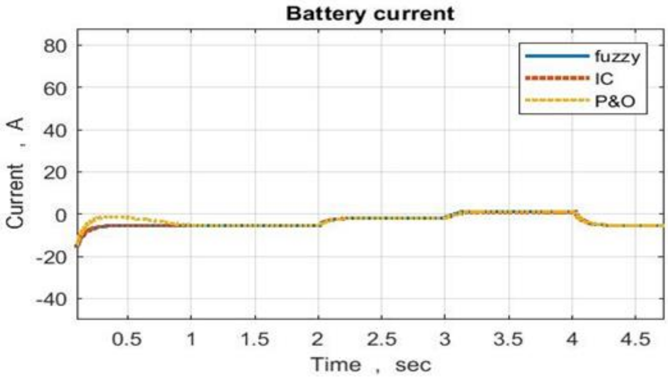

Figure 4.48 Battery current.

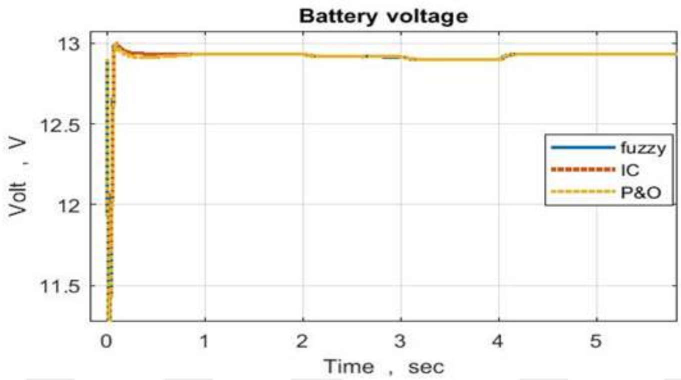

Figure 4.49 Battery voltage.

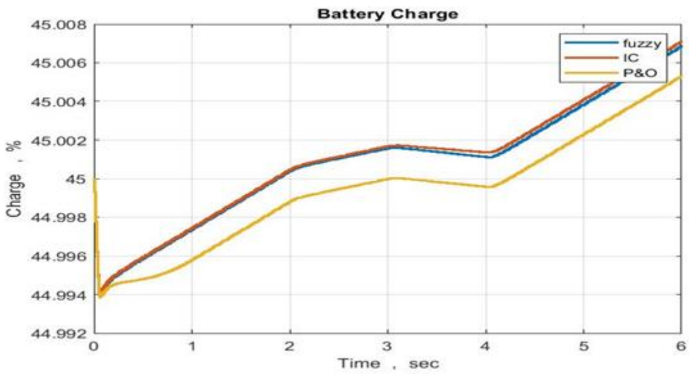

Figure 4.50 Battery charge.

5 RESULTS AND DISCUSSION

A PV system has been designed as shown in Figure 4.39 in MATLAB/Simulink. The numerical values of system parameters can be included in the Table 1, The proposed system consists of a unique PV panel 213 W, model 1Sollech 1STH-215-P, a DC-DC buck converter operates at 10 KHz to charge a battery 12V, and a PI controller is used to control the charge of battery. To operate the system of PV at the maximum power point, three MPPT methods P&O, IC, and FLC are employed. The optimum values of DC-DC parameters have been modified based on the try and error but it strongly depended on the conventional equations mentioned earlier in the part 3.

Table 5.1 The numerical values used in the simulation design

System	Parameter	Symbol	Value
SPV	Maximum power	P_m	213W
	Voltage at maximum power	$V_m = V_{in}$	29 V
	Current at maximum power	$I_m = I_{in}$	7.35A
	Open circuit voltage	V_{oc}	36.3V
	Short circuit current	I_{sc}	7.84A
	Number of cells per module	N_{cell}	60
	Number of cells in series	N_s	1
	Number of cells in parallel	N_p	1
DC-DC converter	Switching frequency	f_{sw}	10 KHz
	Output voltage	V_o	14V
	Output current	I_o	11.6A
	Input current ripple	ΔI_{in}	2% of I_{in}
	Input voltage ripple	ΔV_{in}	0.2% of V_{in}
	Output current ripple	ΔI_o	4% of I_o
	Output voltage ripple	ΔV_o	0.2% of V_o
	Input capacitor	C_{in}	750μF
	Output capacitor	C_o	750μF
	Inductor	L	1.2mH
	Load resistance	R_{load}	1.5Ω
Battery	Battery voltage	V_b	12V
	Rated capacity	$-$	50Ah
	Initial state of charge	SoC	45%
PI controller	Proportional gain	K_p	0.85
	Integral gain	K_i	10

The time of the transient process obtained using the “Perturbation and Observation” algorithm is ≈ 0.8 sec. Power ripples of about 1–2% are observed. This algorithm is very simple to implement and does not require large computational costs. It should also be noted that with a sharp increase or decrease in radiation (during the implementation of the tracking mode or with a sharp change in weather conditions), these algorithms can lose MPPT, so the efficiency can drop by 10–12%.

When the algorithm "Increasing conductivity" is running, the transient process lasts approximately 0.1 s, ripples are about 4-5%. The disadvantage of these schemes is pulsations, which are a consequence of the operation of the algorithms themselves, since the desired value always fluctuates around the MPPT.

The controller based on fuzzy logic does not require the construction of accurate mathematical models of the object, and also allows you to work with nonlinearities. With this implementation, the algorithm provides greater accuracy and speed. MPPT is always achieved, there are practically no pulsations. Efficiency increases up to 3-10 % if compared to previous algorithms. The main disadvantage of using a controller based on fuzzy logic is a non-trivial setting for a specific object. Table 5.2 shows the system control parameters using the different control algorithms.

Table 5.2 MPPT algorithms comparision

	Without MPPT	**P&O**	**IC**	**Fuzzy**
	P_PV			
Rise time	5ms	2ms	3ms	1ms
Stable time	infinity	14ms	5ms	4.2ms
Overshooting	x	2.8%	<3%	<2.6%
Static error	24%	<2%	<3%	<1%
	I_PV			
Rise time	2ms	1ms	3ms	6ms
Stable time	10ms	7.3ms	5ms	8.5ms
Overshooting	1%	X	<1%	<1%
Static error	<2%	<2%	<2%	<1%
	V_PV			
Rise time	5ms	800ms	12ms	8ms
Stable time	infinity	3.7s	17ms	9ms
Overshooting	x	<14%	<1%	<13%
Static error	40%	<4%	<3%	<1%

The values of the results that extracted from the designed systems along with changing the value of the radiation, also the efficiency of the systems has domenstrated in the Table 5.3.

Table 5.3 Results comparision of PV systems

System without MPPT							
Irradiation at 25° C	**Vpv(v)**	**Ipv(A)**	**Ppv(w)**	**Vo(v)**	**Io(A)**	**Po(w)**	**Efficiency**
400	20.86	3.117	65.01	11.90	4.441	50.85	78.21%
700	21.33	5.451	116.3	11.93	7.915	92.41	79.41%
1000	21.79	7.782	169.6	12	11.42	137.1	80.84%
System based P&O MPPT							
400	19.06	3.12	59.46	11.89	4.015	47.74	80.29%
700	28.81	5.23	150.7	11.97	10.6	126.9	84.60%
1000	28.87	7.385	213.2	12.04	15.61	187.9	88.13%
Syestem based IC MPPT							
400	29.44	2.932	86.31	11.91	6.461	76.92	89.12%
700	29.32	5.131	150.4	11.95	11.68	139.5	92.75%
1000	29.82	7.394	213.2	12.04	16.34	196.8	92.35%
System Based Fuzzy Logic MPPT							
400	30.27	2.804	84.86	11.89	6.609	78.57	92.59%
700	29.60	5.094	150.8	11.93	11.79	140.7	93.30%
1000	29	7.332	213	12.03	16.35	200	94.00%

As over all, It has been noted that the behavior of system without the MPPT control gives undesired results in terms of system control parameters summarized in the Table 5.2 particularly a static error about 40% and a stable time which gave infinite values for the power and voltage. The Table 5.3 showed the poor for tracking the MPPT for all the values of voltage, current and power. The efficiency of system between 78 – 80 %.

System based MPPT using a modified Perturb and Observe gave better results than system without MPPT technique as shown in the figures and table of comparison mentioned earlier, but still the rise time, stable time and overshooting are high and not reach the aim of design. The technique showed its weakness at the low irradiation values and partial shadow. The efficiency of system between 80 – 88 %.

By using the Incremental Conductance and the Fuzzy Logic techniques based MPPT, they gave the best results in the studying in terms of the parameters measures as well as the desired values of the voltage, the current and the power in terms of their efficiency for tracking the MPPT along with changing the irradiation values. Their efficiency are ideal between 89 – 92 % for IC while for the FLC, it reached between 92 – 94 %. It is worth mentioning that the oscillation into a system based Fuzzy Logic is less if compared with the IC and certainly with the other previous designs too.

6 CONCLUSIONS AND RECOMMENDATION

A system of PV 213 watt has been designed based on the new concepts and research, comparing of performance of all the techniques have been observed after applying four varying states of solar insolation. The modified techniques showed better performance than the old references approach. A Perturb and Observe is the simplest technique and does not very work well at low irradiation. The incremental conductance IC method has no complicated technique like P&O but gave a better result, a new algorithm gave a result very close to the behavior of FLC. The FLC showed the best result among all the used techniques but it is complicated. All the designed systems gave a fixed output voltage.

A bi-directional battery charge is also designed to increase the life cycle of the battery and charging period, this approach will be helpful to decrease the operating of the battery for a long period but it compensates for the decrease of the required output voltage in the state of a lack of radiation applied on the system. Since there is no standard for designing a DC-DC converter with a unique PV panel or groups of them connected in series, parallel or series and parallel in one design, the equations of conventional DC-DC convertor do not give the optimum values of its parameters, that are attributed to varying of PV power from zero to maximum power of selected PV panel, hence in our study, the supplied power is changing from 0 to 213 watt, also the voltage is changing from 0 to Voc, so it leads to instability in switch gate signal D. Also, it is very clear that when connecting a PV system with the battery which considers an unstable load in addition to the load R, and this will lead to non-ideal results if compared with a fixed load. So, our parameter values for the DC-DC converter have been modified based on try and error.

A study will give a good vision for future research.To increase an efficiency, it is possible to work in the future by using an adaptive fuzzy control to increase the yield and improve the control signal, but this method will increase the complexity of the algorithm.

REFERENCES

Abihana, O. A., & Gonzalez, O. R. 1993. Design and Implementation of Fuzzy Logic Controllers. Thesis Final Report, 27 July 1992-1 January 1993.

Abo-Sennah, M. A., El-Dabah, M. A., & Mansour, A. E.-B. 2021. Maximum power point tracking techniques for photovoltaic systems: a comparative study. International Journal of Electrical & Computer Engineering (2088-8708): 11(1).

Ali, M. H. M., Mohamed, M. M. S., Ahmed, N. M., & Zahran, M. B. A. 2022. Comparison between P&O and SSO techniques based MPPT algorithm for photovoltaic systems. International Journal of Electrical & Computer Engineering (2088-8708): 12(1).

Al-Majidi, S. D., Abbod, M. F., & Al-Raweshidy, H. S. 2018. A novel maximum power point tracking technique based on fuzzy logic for photovoltaic systems. International Journal of Hydrogen Energy, 43(31): 14158-14171.

Ansari, A. Q. 1998. The basics of fuzzy logic: A tutorial review. COMPUTER EDUCATION-STAFFORD-COMPUTER EDUCATION GROUP-, 88: 5-8.

Atallah, A. M., Abdelaziz, A. Y., & Jumaah, R. S. 2014. Implementation of perturb and observe MPPT of PV system with direct control method using buck and buck-boost converters. Emerging Trends in Electrical, Electronics & Instrumentation Engineering: An international Journal (EEIEJ), 1(1): 31-44.

Babaa, S. E., Armstrong, M., & Pickert, V. 2014. Overview of maximum power point tracking control methods for PV systems. Journal of Power and Energy Engineering, 2014.

Baharudin, N. H., Mansur, T. M. N. T., Hamid, F. A., Ali, R., & Misrun, M. I. 2017. Topologies of DC-DC converter in solar PV applications. Indonesian Journal of Electrical Engineering and Computer Science, 8(2): 368-374.

Balagurov, M. V., Sidorov, A. V., Korobkov, D. V., Zharkov, M. A., Shtein, D. A., & Bessonov, I. O. 2015. The universal control system for semiconductor converters with PWM. In 2015 16th International Conference of Young Specialists on Micro/Nanotechnologies and Electron Devices (pp. 379-383). IEEE.

Bendib, B., Belmili, H., & Krim, F. 2015. A survey of the most used MPPT methods: Conventional and advanced algorithms applied for photovoltaic systems. Renewable and Sustainable Energy Reviews, 45: 637–648.

Biabani, M. A. K. A., & Ahmed, F. 2016. Maximum power point tracking of photovoltaic panels using perturbation and observation method and fuzzy logic control based method. In 2016 International Conference on Electrical, Electronics, and Optimization Techniques (ICEEOT) (pp. 1614-1620). IEEE.

Chauhan, J., Chauhan, P., Maniar, T., & Joshi, A. 2013. Comparison of MPPT algorithms for DC-DC converters based photovoltaic systems. In 2013 International Conference on Energy Efficient Technologies for Sustainability (pp. 476-481). IEEE.

De Cesare, G., Caputo, D., & Nascetti, A. 2006. Maximum power point tracker for portable photovoltaic systems with resistive-like load. Solar Energy, 80(8): 982–988.

Dhanaraju, K., Srinu, I., & Satyanarayana, K. 2015. Performance Improvement of Fuzzy PID Controller Based Process Control System. In International Journal of Engineering and Advanced Technology (IJEAT) (Issue 6).

Dolara, A., Faranda, R., & Leva, S. 2009. Energy comparison of seven MPPT techniques for PV systems. Journal of Electromagnetic Analysis and Applications, 2009.

Dorofte, C., Borup, U., & Blaabjerg, F. 2005. A combined two-method MPPT control scheme for grid-connected photovoltaic systems. 2005 European Conference on Power Electronics and Applications: 10-pp.

Doubabi, H., Salhi, I., Chennani, M., & Essounbouli, N. 2021. High Performance MPPT based on TS Fuzzy–integral backstepping control for PV system under rapid varying irradiance—Experimental validation. ISA transactions, 118: 247-259.

Elbaksawi, O. 2019. Design of photovoltaic system using buck-boost converter based on MPPT with PID controller. Universal Journal of Electrical and Electronic Engineering, 6(5): 314–322. https://doi.org/10.13189/ujeee.2019.060502

Elgendy, M. A., Zahawi, B., & Atkinson, D. J. 2011. Assessment of perturb and observe MPPT algorithm implementation techniques for PV pumping applications. IEEE Transactions on Sustainable Energy, 3(1): 21–33.

Esram, T., & Chapman, P. L. 2007. Comparison of photovoltaic array maximum power point tracking techniques. IEEE Transactions on Energy Conversion, 22(2): 439–449.

Esram, T., Kimball, J. W., Krein, P. T., Chapman, P. L., & Midya, P. 2006. Dynamic maximum power point tracking of photovoltaic arrays using ripple correlation control. IEEE Transactions on Power Electronics, 21(5) 1282–1291.

Faranda, R., & Leva, S. 2008. Energy comparison of MPPT techniques for PV Systems. WSEAS Transactions on Power Systems, 3(6): 446–455.

Femia, N., Granozio, D., Petrone, G., Spagnuolo, G., & Vitelli, M. 2006. Optimized one-cycle control in photovoltaic grid connected applications. IEEE Transactions on Aerospace and Electronic Systems, 42(3): 954–972.

Femia, N., Petrone, G., Spagnuolo, G., & Vitelli, M. 2005. Optimization of perturb and observe maximum power point tracking method. IEEE Transactions on Power Electronics, 20(4): 963–973.

Haji, D., & Genc, N. 2018. Fuzzy and P&O based MPPT controllers under different conditions. In 2018 7th International Conference on Renewable Energy Research and Applications (ICRERA) (pp. 649-655). IEEE.

Haque, A. 2014. Maximum power point tracking (MPPT) scheme for solar photovoltaic system. Energy Technology & Policy, 1(1): 115-122.

Hsiao, Y. T., & Chen, C. H. 2002. Maximum power tracking for photovoltaic power system. In Conference record of the 2002 IEEE industry applications conference. 37th IAS Annual Meeting (Cat. No. 02CH37344) (Vol. 2, pp. 1035-1040). IEEE.

Ismail, N. N., Musirin, I., Baharom, R., & Johari, D. 2010. Fuzzy logic controller on DC/DC boost converter. In 2010 IEEE International Conference on Power and Energy (pp. 661-666). IEEE.

Jusoh, M. A., Tajuddin, M. F. N., Ayob, S. M., & Roslan, M. A. 2018. Maximum power point tracking charge controller for standalone PV system. Telkomnika (Telecommunication, Computing, Electronics and Control), 16(4): 1413-26.

Karlsson, B., Rúben, M. M., & Fonseca Batista, V. 2018. The impact of shadowing in photovoltaic systems and how to minmize it an analysis with the pv system software. Energy Systems Master Programme in Energy Systems.

Kato, K., & Koizumi, H. 2015. A study on effect of blocking and bypass diodes on partial shaded PV string with compensating circuit using voltage equalizer. 2015 IEEE International Symposium on Circuits and Systems (ISCAS): 241–244.

Kchaou, A., Naamane, A., Koubaa, Y., & M'Sirdi, N. K. 2016. Comparative study of different MPPT techniques for a stand-alone PV system. In 2016 17th International Conference on Sciences and Techniques of Automatic Control and Computer Engineering (STA) (pp. 629-634). IEEE.

Kobayashi, K., Matsuo, H., & Sekine, Y. 2004. A novel optimum operating point tracker of the solar cell power supply system. 2004 IEEE 35th Annual Power Electronics Specialists Conference (IEEE Cat. No. 04CH37551), 3: 2147–2151.

Kottas, T. L., Boutalis, Y. S., & Karlis, A. D. 2006. New maximum power point tracker for PV arrays using fuzzy controller in close cooperation with fuzzy cognitive networks. IEEE Transactions on Energy Conversion, 21(3): 793–803.

Koutroulis, E., & Blaabjerg, F. 2012. A new technique for tracking the global maximum power point of PV arrays operating under partial-shading conditions. IEEE Journal of Photovoltaics, 2(2): 184–190.

Lee, J. H., Bae, H., & Cho, B. H. 2006. Advanced incremental conductance MPPT algorithm with a variable step size. 2006 12th International Power Electronics and Motion Control Conference, 603–607.

Leedy, A. W., Guo, L., & Aganah, K. A. 2012. A constant voltage MPPT method for a solar powered boost converter with DC motor load. 2012 Proceedings of IEEE Southeastcon, 1–6.

Lopez-Lapena, O., & Penella, M. T. 2012. Low-power FOCV MPPT controller with automatic adjustment of the sample&hold. Electronics Letters, 48(20): 1301–1303.

Mahalakshmi, R., Kumar, A., & Kumar, A. 2014. Design of Fuzzy Logic based Maximum Power Point Tracking controller for solar array for cloudy weather conditions. In 2014 Power and Energy Systems: Towards Sustainable Energy (pp. 1-4). IEEE.

Murtaza, A. F., Sher, H. A., Chiaberge, M., Boero, D., De Giuseppe, M., & Addoweesh, K. E. 2013. Comparative analysis of maximum power point tracking techniques for PV applications. In Inmic (pp. 83-88). IEEE.

Narendiran, S. 2013. Grid tie inverter and MPPT-A review. 2013 International Conference on Circuits, Power and Computing Technologies (ICCPCT): 564–567.

Narendiran, S., Sahoo, S. K., Das, R., & Sahoo, A. K. 2016. Fuzzy logic controller based maximum power point tracking for PV system. In 2016 3rd International Conference on Electrical Energy Systems (ICEES) (pp. 29-34). IEEE.

Ngan, M. S., & Tan, C. W. 2011. A study of maximum power point tracking algorithms for stand-alone photovoltaic systems. In 2011 IEEE Applied Power Electronics Colloquium (IAPEC) (pp. 22-27). IEEE.

Noman, A. M., Addoweesh, K. E., & Mashaly, H. M. 2012. A fuzzy logic control method for MPPT of PV systems. In IECON 2012-38th Annual Conference on IEEE Industrial Electronics Society (pp. 874-880). IEEE.

Pandey, A., Dasgupta, N., & Mukerjee, A. K. 2007. A simple single-sensor MPPT solution. IEEE Transactions on Power Electronics, 22(2): 698–700.

Park, M., & Yu, I.-K. 2004. A study on the optimal voltage for MPPT obtained by surface temperature of solar cell. 30th Annual Conference of IEEE Industrial Electronics Society, 2004. IECON 2004, 3: 2040–2045.

Patel, H., & Agarwal, V. 2008. Maximum power point tracking scheme for PV systems operating under partially shaded conditions. IEEE Transactions on Industrial Electronics, 55(4): 1689–1698.

Pathak, P. K., & Yadav, A. K. 2019. Design of battery charging circuit through intelligent MPPT using SPV system. Solar Energy, 178: 79–89.

Rebhi, M., Benatillah, A., Sellam, M., & Kadri, B. 2013. Comparative study of MPPT controllers for PV system implemented in the south-west of Algeria. Energy Procedia, 36: 142–153.

Sahin, M. E., & Okumus, H. İ. 2011. Fuzzy logic controlled buck-boost DC-DC converter for solar energy-battery system. In 2011 International Symposium on Innovations in Intelligent Systems and Applications (pp. 394-397). IEEE.

Salas, V., Olias, E., Barrado, A., & Lazaro, A. 2006. Review of the maximum power point tracking algorithms for stand-alone photovoltaic systems. Solar Energy Materials and Solar Cells, 90(11): 1555–1578.

Salas, V., Olias, E., Lazaro, A., & Barrado, A. 2005. New algorithm using only one variable measurement applied to a maximum power point tracker. Solar Energy Materials and Solar Cells, 87(1–4): 675–684.

Salman, S., Xin, A. I., & Zhouyang, W. U. 2018. Design of a P-&-O algorithm based MPPT charge controller for a stand-alone 200W PV system. Protection and Control of Modern Power Systems, 3(1): 1-8.

Selvan, S., & Kumar, G. 2015. Comparative study of perturb & observe and fuzzy logic control based MPPT algorithms. International Journal of Advances in Engineering & Technology, 7(6): 1649.

Sera, D., Kerekes, T., Teodorescu, R., & Blaabjerg, F. 2006. Improved MPPT method for rapidly changing environmental conditions. 2006 IEEE International Symposium on Industrial Electronics, 2: 1420–1425.

Sharma, C., & Jain, A. 2014. SIMULATION OF BUCK, BOOST AND BUCK-BOOST POWER CONVERTERS FOR SOLAR PANEL

Sharma, C., & Jain, A. 2015. Modeling of Buck Converter Models in MPPT using PID and FLC. TELKOMNIKA, 13(4): 1270.

Sharma, C., & Jain, A. 2015. Performance comparison of PID and fuzzy controllers in distributed MPPT. International Journal of Power Electronics and Drive Systems (IJPEDS), 6(3): 625-635.

Singh, P., Shukla, N., & Gaur, P. 2021. Modified variable step incremental-conductance MPPT technique for photovoltaic system. International Journal of Information Technology, 13(6): 2483-2490.

Sivanandam, S. N., Sumathi, S., & Deepa, S. N. 2007. Introduction to fuzzy logic using MATLAB (Vol. 1). Berlin: Springer.

Tajuddin, M. F. N., Arif, M. S., Ayob, S. M., & Salam, Z. 2015. Perturbative methods for maximum power point tracking (MPPT) of photovoltaic (PV) systems: a review. International Journal of Energy Research, 39(9): 1153–1178.

Tremblay, O., & Dessaint, L. A. 2009. Experimental validation of a battery dynamic model for EV applications. World electric vehicle journal, 3(2): 289-298.

Tremblay, O., Dessaint, L. A., & Dekkiche, A. I. 2007. A generic battery model for the dynamic simulation of hybrid electric vehicles. In 2007 IEEE Vehicle Power and Propulsion Conference (pp. 284-289). Ieee.

Tse, K. K., Chung, H. S. H., Hui, S. Y. R., & Ho, M. T. 2001. A novel maximum power point tracking technique for PV panels. In 2001 IEEE 32nd Annual Power Electronics Specialists Conference (IEEE Cat. No. 01CH37230) (Vol. 4, pp. 1970-1975). IEEE.

Xiong, Y., Qian, S., & Xu, J. 2012. Research on constant voltage with incremental conductance MPPT method. 2012 Asia-Pacific Power and Energy Engineering Conference, 1–4.

Yilmaz, U., Kircay, A., & Borekci, S. 2018. PV system fuzzy logic MPPT method and PI control as a charge controller. Renewable and Sustainable Energy Reviews, 81: 994-1001.

Zhang, X., Zhang, H., Zhang, H., Zhang, P., Wang, F., Jia, H., & Song, D. 2016. A variable step-size P&O method in the application of MPPT control for a PV system. In 2016 IEEE Advanced Information Management, Communicates, Electronic and Automation Control Conference (IMCEC) (pp. 1503-1506). IEEE.

Zhou, S., Kang, L., Sun, J., Guo, G., Cheng, B., Cao, B., & Tang, Y. 2010. A novel maximum power point tracking algorithms for stand-alone photovoltaic system. International journal of control, automation and systems, 8(6): 1364-1371.

APPENDICES

APPENDIX 1. P&O algorithm matlab code

APPENDIX 2. IC algorithm matlab code

APPENDIX 3. Parmeters of PV matlab code

APPENDIX 4. Figures matlab code

APPENDIX 1. P&O algorithm matlab code

```
function D = DutyRatio(V, I)

Dmax = 0.95;
Dmin = 0;
Dinit = 0.95;
deltaD = 0.0001;
persistent Vold Pold Dold;

dataType = 'double';

if isempty(Vold)
    Vold = 0;
    Pold = 0;
    Dold = Dinit;
end

P = V*I;
dV = V-Vold;
dP = P-Pold;

if dP ~= 0
    if dP<0
        if dV<0
            D = Dold - deltaD;
        else
            D = Dold + deltaD;
        end
    else
        if dV<0
            D = Dold + deltaD;
        else
            D = Dold - deltaD;
        end
    end
else D = Dold;
end

if D >= Dmax || D <= Dmin
    D = Dold;
end

Dold =D;
Vold = V;
Pold = P;
```

APPENDIX 2. IC algorithm MATLAB code

```
function y = MYMPP (u,i,uo,io,D)
m = 0.4310;
du = u - uo;
di = I - io;
d = 0.05;

if du == 0
    if di == 0
    D = m;

    else

        if di>0
            D = m - d;

        else
            D = m + d;
        end
    end
else

    if di/du == -(i/u)

    D = m;

    else
        if di/du> -(i/u)

        D = m - d;

        else

            D = m + d;
        end
    end
end

y = D;

end
```

APPENDIX 3. Parmeters of PV matlab code

```
Ts=1e-5; %Sampling time
P=213; %Rated power
mppt=readfis('mppt3.fis')
% Design of buck Converter
Vmpp=29;
Vin=Vmpp; %input voltage of buck converter
Vo=14;
n=1;
fs=5e3; %swiching frequencyIL=P/Vin;
Io= P/Vo;
IL=P/Vin;
Io_ripple=0.02*IL;
Vo_ripple=Vo/100;
D=Vo/Vin;
L=Vo*(Vin-Vo)/(Io_ripple*fs*Vin);
C=Io_ripple/(8*fs*Vo_ripple);
```

APPENDIX 4. Figures matlab code

```
D= 29 / 14;
L=0.0019;
C=0.0001469;
R=1.5;
s=tf('s');
H=(D/(L*C))/(s^2+s/(L*C) + 1/(L*C));
figure (1);
step(H);
figure (2);
bode(H);

%% PV Power
figure (3);
plot (Ppv_fuzzy);
hold on;
plot (Ppv_IC);
hold on;
plot (Ppv_PO);
title ('PV power using MPPT algorithms');
legend('fuzzy','IC','P&O');
xlabel ('Time, sec');
ylabel ('Power, W');
grid on;

%% PV voltage
figure (4)
plot (Vpv_fuzzy)
hold on;
plot (Vpv_IC);
hold on;
plot (Vpv_PO);
title ('PV voltage using MPPT algorithms');
legend('fuzzy','IC','P&O');
xlabel ('Time, sec');
ylabel ('Volt, V');

%% PV current
figure (5);
```

```
plot (Ipv_fuzzy);
hold on;
plot (Ipv_IC);
hold on;
plot (Ipv_PO);
title ('PV current using MPPT algorithms');
legend ('fuzzy','IC','P&O');
xlabel ('Time, sec');
ylabel ('Current, A');
grid on;

%% Output Power
figure (6);
plot (Po_fuzzy);
hold on;
plot (Po_IC);
hold on;
plot (Po_PO);
title ('O/P power using DC_DC Buck Convertor');
legend('fuzzy','IC','P&O');
xlabel ('Time, sec');
ylabel ('Power, W');
grid on;

%% Output voltage
figure (7)
plot (Vo_fuzzy)
hold on;
plot (Vo_IC);
hold on;
plot (Vo_PO);
title ('O/P voltage using DC_DC Buck Convertor');
legend('fuzzy','IC','P&O');
xlabel ('Time, sec');
ylabel ('Volt, V');

%% Output current
figure (8);
plot (Io_fuzzy);
```

```
hold on;
plot (Io_IC);
hold on;
plot (Io_PO);
title ('O/P current using DC_DC Buck Convertor');
legend('fuzzy','IC','P&O');
xlabel ('Time, sec');
ylabel ('Current, A');
grid on;


%% Battery voltage
figure (9)
plot (Bat_volt_fuzzy)
hold on;
plot (Bat_volt_IC);
hold on;
plot (Bat_volt_PO);
title ('Battery voltage');
legend('fuzzy','IC','P&O');
xlabel ('Time, sec');
ylabel ('Volt, V');

%% Battery current
figure (10);
plot (Bat_current_fuzzy);
hold on;
plot (Bat_current_IC1);
hold on;
plot (Bat_current_PO);
title ('Battery current');
legend('fuzzy','IC','P&O');
xlabel ('Time, sec');
ylabel ('Current, A');
grid on;
```

CURRICULUM VITAE

Personal Information

Name and Surname : Ahmed AL-JABARI

Education

MSc	Çankırı Karatekin University Graduate School of Natural and Applied Sciences Department of Chemical Engineering	2019-Present
Undergraduate	Tikrit University Faculty of Engineering Department of Electrical Engineering	2005-2008

Academic Activities

1. Al-Jabari, A.R., Korkmaz, F., and Teke, M. (2022). A simulation of stand-alone solar energy system controlled by P&O, IC, and Fuzzy Logic using bidirectional charging of battery. KJE.